National Radio Astronomy Observatory
Green Bank, West Virginia
ELECTRONICS DIVISION INTERNAL REPORT NO. 316

A Study of Radar Signals Received by the Green Bank Telescope

J. R. Fisher, A. Singhal

May 8, 2006

1 Introduction

The strongest interfering signals received in the passband of the Green Bank Telescope's (GBT) 1.15-1.7 GHz receiver are radar pulses at 1256 and 1292 MHz. These pulses are transmitted by an ARSR-3 FAA Air Surveillance Radar on Apple Orchard Mountain near Bedford, VA, longitude 79.510W, latitude 37.517N, elevation 1288 meters (4225 feet). This radar antenna is about 106 km south-southeast of the GBT at an azimuth of 164 degrees. The radar transmits a 2-microsecond pulse with an average repetition rate of 341 pulses per second. The radar antenna has an azimuthal beamwidth of about 1 degree and an azimuthal sweep rate of 5 rpm (12 second rotation period). When the radar beam is pointed near the direction of the GBT the 1.15-1.72 GHz Gregorian receiver is saturated during the radar pulse unless a notch filter is inserted after the cooled RF amplifiers.

This report presents the results of a study of the characteristics of the received radar signals and what can be learned from them about the propagation of RFI in the mountainous terrain surrounding Green Bank. Long-delay echoes from aircraft and rain showers are shown. These results are then used to develop and test algorithms for removing the radar signals from the receiver output so that astronomical observations can be made at the frequencies of the radar signals.

2 Path Loss and Signal Strength

The radar transmitter has a peak power of about 2 megawatts in a 2-microsecond pulse, and the radar antenna gain is about 35 dBi. The computed direct path loss from the radar to the GBT focal point calculated with he NRQZ propagation model is 183 dB so the received field strength at each radar frequency is about -61 dBW/m^2. With an estimated GBT far sidelobe gain of -15 dBi the peak signal strength at the first RF amplifier input is calculated to be -70 dBm. This agrees quite well with the peak power value of -75 dBm at the input to this receiver measured by [Stennes (2001)].

3 Data Acquisition

The data described in this report are from eight measurement sessions between February 2001 and April 2003. The parameters for each session are given in Table 1. The first session recorded the signal from the GBT's 1.15-1.72 GHz receiver with the GBT in service position (pointing near the zenith). The last session used the GBT to record an extensive integration on the galaxy UGC 4288 whose neutral hydrogen (HI) spectrum is redshifted to near the 1292 MHz radar signal. All other sessions used a 1.2-1.7 GHz sectoral horn mounted about 7 meters above the ground on the RFI monitor station (locally referred to as the "deer

Table 1: Parameters for the five data acquisition sessions.

Date	Signal Source	Ctr Freq (MHz)	Bandw (MHz)	Sample Rate (MS/s)	Sampler Type	Duration (Sec.)	Purpose
Feb. 06, 2001	GBT	1292.93	10.0	20 000	Signatec	3 x 5	Init. trial
Mar. 25, 2002	RFI Monit.	1292.85	3.0	10.818	Signatec	17 x 2.9	Var. Gain/Az
Mar. 26, 2002	RFI Monit.	1292.85	3.0	10.818	Signatec	16 x 5.8	Rain
Apr. 05, 2002	RFI Monit.	1292.85	3.0	10.818	Signatec	4 x 5.8	Aircraft
Feb. 02, 2003	RFI Monit.	1292.00	5.0	10.000	ADLink	600	Aircraft
Mar. 31, 2003	GBT	1290.69	5.0	10.000	ADLink	600	UGC 4288
Apr. 01, 2003	GBT	1290.69	5.0	10.000	ADLink	600	UGC 4288
Apr. 17, 2003	GBT	1293.54	5.0	10.000	ADLink	600	1007+0121

stand") just west of the works area gate. The GBT system temperature was about 20 Kelvin, and its effective gain is roughly estimated to be -15 dBi in the direction of the horizon. The sectoral horn system temperature was about 400 Kelvin, its maximum gain was about +10 dBi, and its 3-dB beamwidth was about 50 degrees. This horn could be remotely controlled to point to any azimuth.

In all sessions the recorded data were 8-bit A/D samples of IF amplifier output voltages with sample rates greater than or equal to twice the band-limiting filter bandwidth. In every case the bandpass included only the 1292 MHz radar frequency. In the Feb. 6, 2001 and all 2003 recording sessions the IF outputs were from the spectral processor IF system which presents a low-pass filtered baseband signal to the A/D sampler. The other sessions used a final bandpass filter with a center frequency of 30 MHz and a 3-dB bandwidth of 3 MHz. When the 30 MHz filter was used a sampling rate of 10.81818 MS/s was chosen so that the fifth sampling alias (zeroth alias = baseband) fell between 27.04545 and 32.45455 MHz. These frequencies were close to the 10-dB attenuation levels of the filter skirts. With the exception of the Feb. 6, 2001 and Apr. 1, 2003 data, increasing baseband frequency corresponds to increasing frequency at the antenna.

The Signatec A/D sampler was a PDA500 high-speed sampler board running under the MS Windows operating system. This system had the unfortunate habit of dropping two or three microseconds of data at irregular intervals of about one second. This became evident in measured radar pulse arrival times, and the only way to compensate for these data gaps was to visually inspect the data sets for jumps in the pulse timing and compile a table of data gap times and durations for use in subsequent data analysis. The ADLink PCI9812 data acquisition board, running under Linux, did not suffer from this problem.

The ADLink PCI9812 is a 12-bit A/D board, but only the central 8 bits were recorded to conserve disk space and to maximize the sampling rate that could be continuously streamed to disk. Bits 2:9 out of 0:11 were chosen by inspection of the 4098 sampling levels with a smooth sine wave input. The sampling levels showed random amplitude errors on the order of 10% of the spacing between levels, and dropping the two lowest order bits reduced the fractional random error of the smallest sampling interval by about a factor of four. A slight jump (much less than one sampling interval) in the A/D transfer function was also seen between levels 255 and 256 (between bits 7 and 8). Hence, this glitch was between recorded levels 63 and 64 (between bits 5 and 6), which was higher than most of the data sample amplitudes recorded in these measurements. The Signatec PDA500 data acquisition board showed sampling level errors up to 50% of the sampling interval, but, since it was an 8-bit A/D, all of its output bits were recorded. The available test sine waveform was not accurate enough to measure large scale non-linearities in the A/D transfer functions. None of these errors had any substantial effect on the results to follow in this report.

The recorded samples from the PDA500 board were unsigned integers with zero volts input producing an output value of about 127. The average offset of these data values was subtracted from all sample values to produce a zero-mean signed value for further processing. The PCI9812 produced signed integers with nearly zero mean.

Using white, band-limited noise from RF amplifiers as input to the A/D sampler boards the ADLink PCI9812 showed no spectral features that might be attributed to internally generated digital noise after a few hundred seconds of integration. The Signatec PDA500 produced spurious spectral features below a few

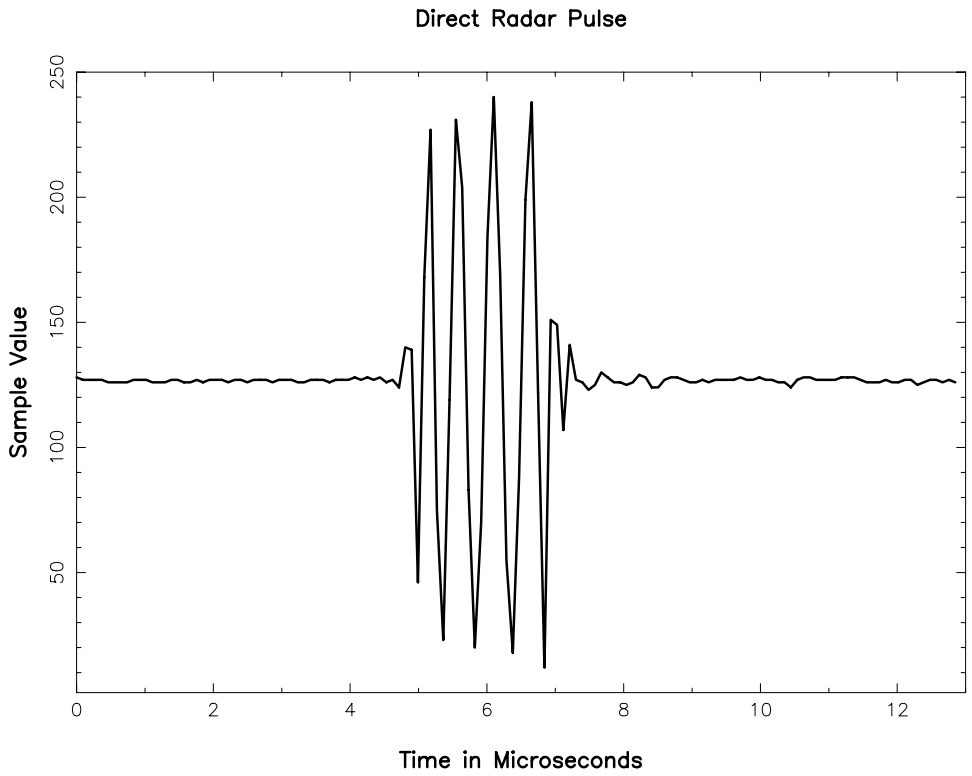

Figure 1: Strong radar pulse received with the sectoral horn pointed to the radar and the radar beam nearly pointed at Green Bank. A 20 dB attenuator was inserted after the antenna preamp to avoid saturating later RF stages.

hundred kilohertz that were evident in less that one second of integration. Since these spurious signals did not overlap with the radar signals of interest their spectral channels were discarded and had no effect on the results.

The sampling clocks for the A/D boards were derived from the site clock based on a hydrogen maser, which was stable to better than one part in 10^{12}. The one exception to this was the first, Feb. 6, 2001, session, which used the internal computer clock. This clock drifted few hundred microseconds with respect to atomic time in the five-second data recordings. This drift was well characterized by a sixth-order polynomial equation and was removed from the timing results.

4 Pulse Shape and Spectrum

Figure 1 shows the data sample segment around an isolated, strong radar pulse. The computed spectrum of this pulse is shown in Figure 2. The measured radar carrier frequency is close to 1292.15 MHz, and the higher-frequency sidebands are due to the intentionally square pulse shape. A good estimate of the shape of the pulse amplitude envelope may be computed by taking the real-to-complex discrete Fourier transform (DFT) of the pulse data samples to obtain the complex spectrum, then computing the inverse DFT of this spectrum to get complex data samples equivalent to the original data. Figure 3 shows the result of this computation for two successive pulses. The pulses are broadened slightly because of the IF filter roll-off of -10 dB at the edges of the spectrum shown in Figure 2.

The signal-to-noise ratio of the received radar pulses can be enhanced by filtering the data to exclude all of the passband except that which contains radar power. A matched filter is one whose frequency structure is the complex conjugate of the measured radar pulse spectrum. A simpler filter is one that approximates just the main spectral feature at 1292.15 MHz shown in Figure 2. A gaussian with a half-power width of 0.5

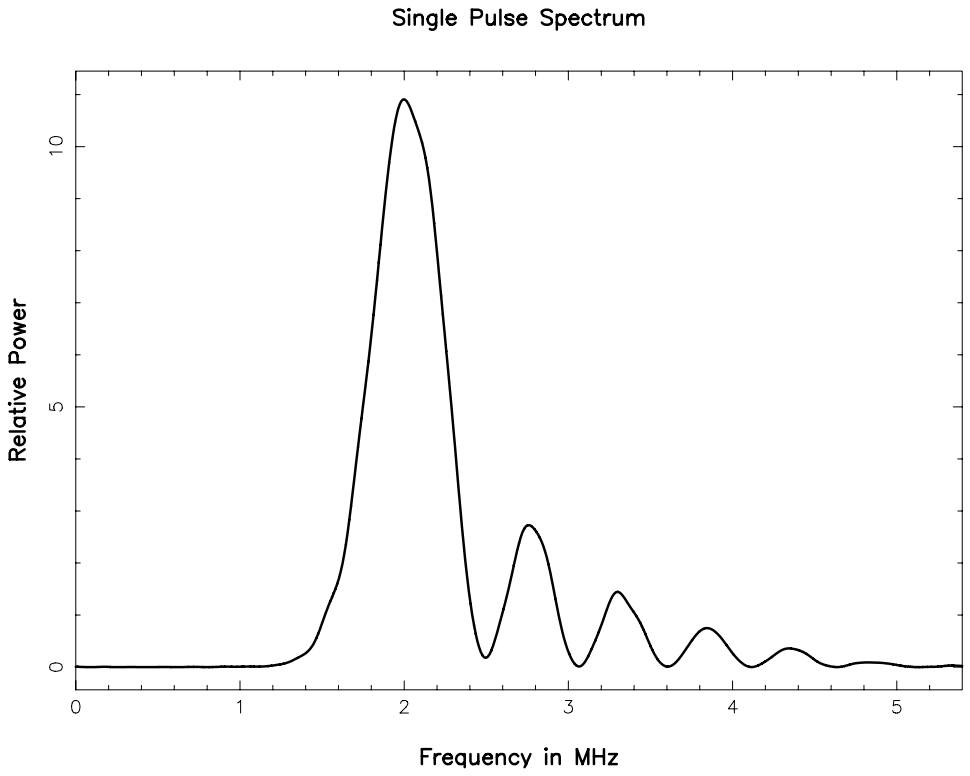

Figure 2: Spectrum of pulse shown in Figure 1 computed from its Fourier transform. The first receiver L.O. frequency was 1322.6 MHz, and zero frequency in the spectrum corresponds to the edge of the sampling alias window at 32.45455 so that 0.0 MHz in this spectrum is 1290.1455 MHz, and 5.0 MHz is 1295.1455 MHz at the antenna.

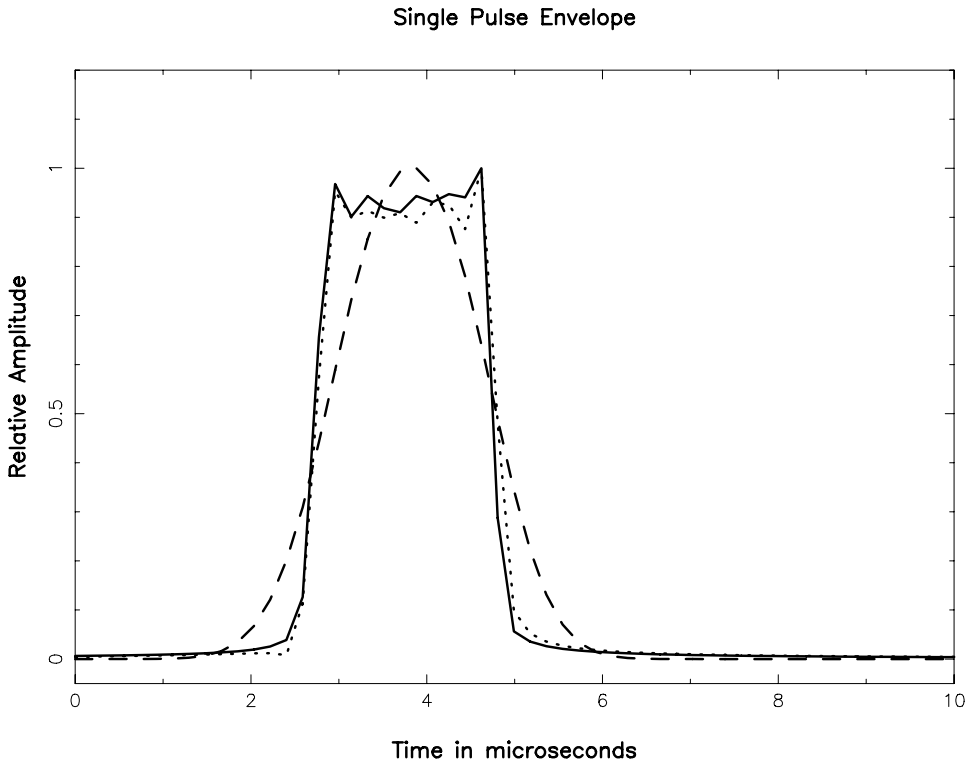

Figure 3: Computed pulse amplitude envelope for the pulse shown in Figure 1 (solid line). The envelope of the next following pulse is plotted as the dotted curve to show the pulse-to-pulse consistency. The envelopes have been scaled to a peak value of 1.0 for comparison. The dashed curve shows the effective pulse envelope that results from filtering the radar spectrum with a gaussian filter shape that closely approximates the main spectral feature in Figure 2. The horizontal scale zero point is arbitrary

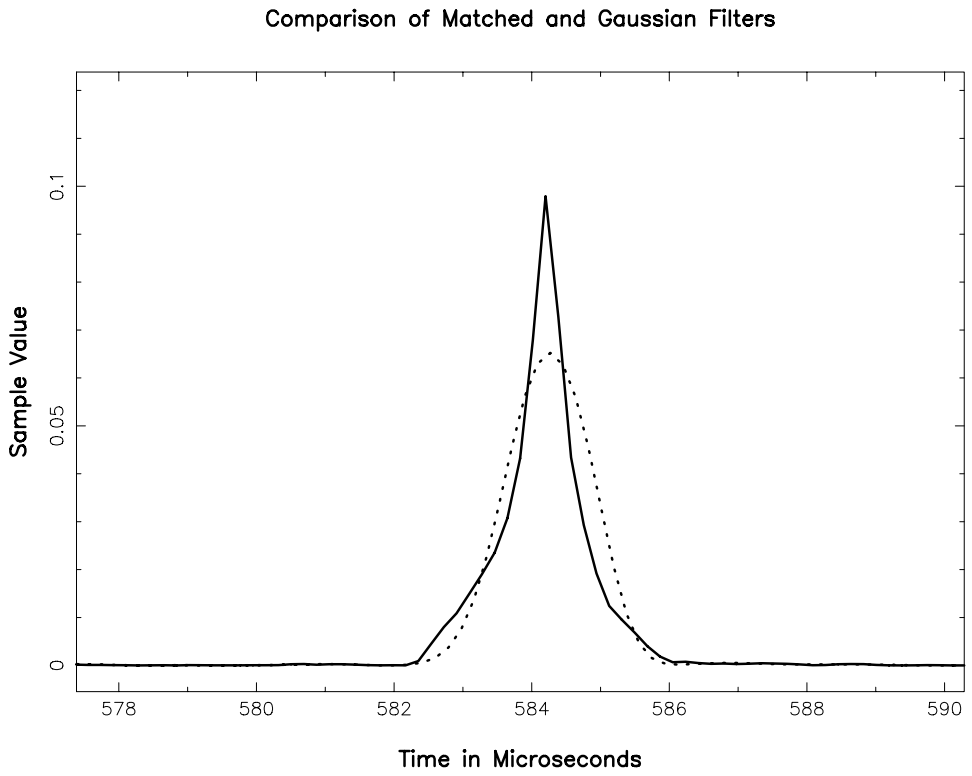

Figure 4: Isolated radar pulse received from an aircraft reflection with the data processed with a filter matched to the square pulse shown in Figure /refpulseenv (solid curve) and with a 0.5 MHz half-power gaussian filter (dotted curve). The amplitudes have been scaled for equal average noise powers at delays where there are no pulses received. The time scale zero point is arbitrary.

MHz is quite close. The simpler filter is more useful when the measured spectrum does not include the radar sidebands. Figure 4 shows an isolated pulse received from an aircraft reflection that has been filtered with both a matched and a gaussian filter. The data have been scaled so that the average off-pulse noise powers are the same. The matched filter provides a higher measured peak power and slightly higher time resolution as one would expect from using all of the received pulse information. The time profile of a matched filter response to a square pulse is a triangle squared, which is roughly what is seen in Figure 4. Figure 5 compares the output of the two filters at a delay where many reflections are seen from local terrain. In this case the advantages of the matched filter are not as clear. Unless otherwise noted, all data analysis in this report used the simpler gaussian filter.

5 Pulse Timing

Pulse timing parameters of the radar might have been obtained from the transmitting facility personnel, but these parameters can also be measured from the received signal. The iterative, manual process used to determine the radar's timing and transmission characteristics was a bit tedious and indirect, but it was a good way to discover and understand some unanticipated effects. Hence, the process will be described in same detail.

The first step was to filter the data with a gaussian filter in the frequency domain that matched the main radar spectral feature shown in Figure 2. This was done by Fourier transforming 2048 data samples at a time into complex 1024-point frequency spectrum. This spectrum was then multiplied by the filter function whose center frequency and bandwidth were adjusted to the frequency scale of the acquired data set. The filtered spectrum was then Fourier transformed back to the time domain where the 1024-point complex time

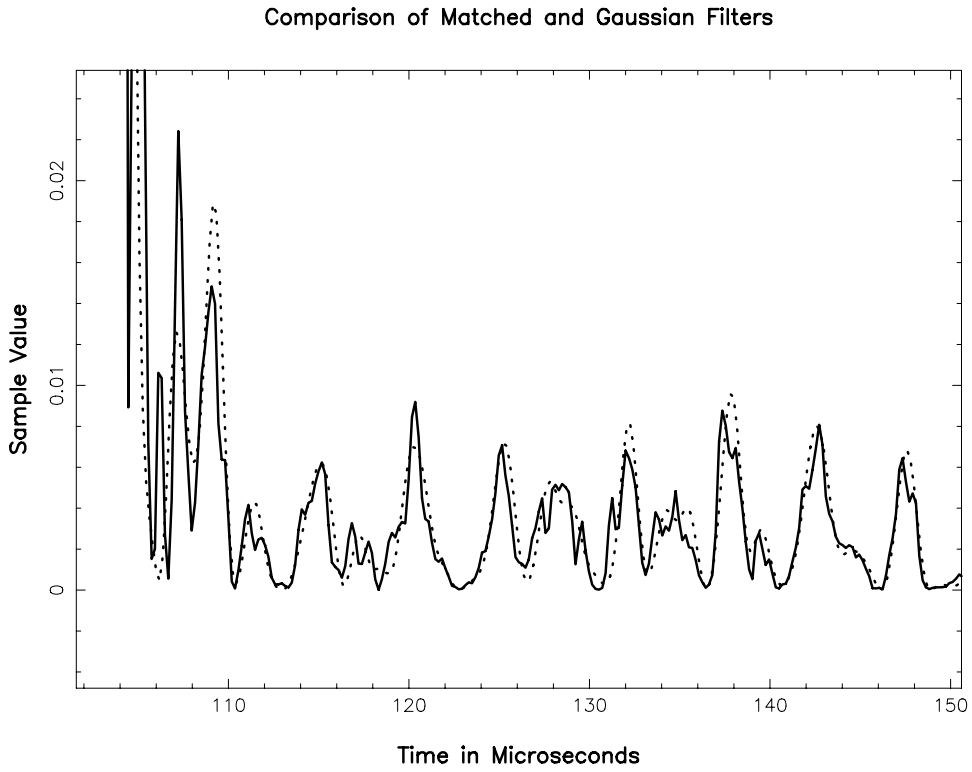

Figure 5: Radar pulse received from local terrain reflections at various delays with the data processed by a filter matched to the square pulse shown in Figure 3 (solid curve) and by a 0.5 MHz half-power gaussian filter (dotted curve). The amplitudes have been scaled for equal average noise powers at delays where there are no pulses received. The time scale zero point is arbitrary.

samples were multiplied by their complex conjugates to produce an array of measured power values as a function of time at half of the original sampling rate. The output data were four-byte floating point to avoid concerns of overflow and quantization error.

Since the data were processed piecemeal in blocks of 2048 samples one worries the the doubly transformed and decimated data my not be an accurate representation of the original samples, particularly near the splice points of the blocks. This was checked by processing overlapping blocks and looking to see how well the processed overlapping data values matched. The match was very good for all but a few end points so the data were processed in block that overlapped by 64 original data samples, and 4 filtered and decimated points were dropped from either end of the processed data blocks.

A note in passing is that a real-valued filter function applied to the complex spectrum caused no time shift in the re-transformed time series, but the complex filter function derived from the measured square pulse did. This is because the square-pulse filter function had a phase slope across its passband that is equivalent to a delay in the time domain. This phase slope could be removed from the filter function before applying it.

The radar pulse spacing is not constant but follows a repeating sequence of 8 pulse spacings around a nominal value of about 2.929 milliseconds. This variable spacing is presumably intended to avoid possible ambiguities from reflections with delays greater than the spacing between pulses.

Determining the transmitted pulse spacing is a bit tricky because, as will be illustrated later, the copy of a pulse arriving by way of the direct path from the radar may be weaker than the same pulse reflected from local terrain. In fact, when the radar beam is pointed to a strong local terrain reflection point the direct path pulse may not be detectable. Hence, some care needs to be exercised to choose data taken while the radar beam in in a position where the direct pulse is clearly detected. If pulse synchronization is to be automated in an RFI blanker system, a receiving antenna that is directional enough to discriminate against delayed arrival paths needs to be used.

The first step in determining the radar parameters is to measure the pulse spacing sequence. This can be done roughly by visual inspection of the data, but a more accurate algorithm was developed to scan an entire data file of at least a few seconds duration and measure the first times of arrival of all detected pulses. After some experimentation the pulse detection threshold was set to 18 times the 90th percentile filtered data power value. This minimized false detections and assured that the pulses were strong enough to make an accurate time-of-arrival measurement. The full data set was scanned sequentially to look for excursions above the detection threshold. When one was found the algorithm stepped forward to the next peak by looking for the next decrease in intensity. A parabola was fit to the three data values around this peak, and the position of the parabola axis was taken as the pulse arrival time. The search was then resumed 500 microseconds after this measured time to avoid detecting pulse echoes from nearby terrain. All spacings between adjacent detected pulses were recorded in a text file and plotted in a frequency-of-occurrence histogram, such as the one in Figure 6.

Figure 6 shows that there are eight dominant pulse spacing in the data set ranging from about 2500 to 3400 microseconds. None of the spacings appear to be repeated since none of the peaks are twice the average frequency of occurrence. False detections and spacings between pulse echoes instead of the directly received pulses are scattered around at other spacings in Figure 6. Figure 7 shows an expanded plot of the pulse spacing distribution around 2533 microseconds and illustrates that the determination pulse timing is accurate to about 0.2 microseconds when a good direct pulse is detected. The measured pulse spacing from Figure 6 are 2533.65, 2632.50, 2731.33, 2830.25, 3028.03, 3126.85, 3225.75, and 3324.62 microseconds. The average spacing is 2929.122 microseconds which gives an average pulse repetition rate of 341.39917 pulses per second. In principle, it should be possible to refine the accuracy of the average repetition rate by dividing the difference in arrival times of pulses near either end of the data set, by the integer number of pulses between them, but this proved problematic because of the difficulty of seeing the direct-arrival pulse over much of the radar sweep. A more interactive way of refining the repetition rate is described later in Section 6.

Figure 6 does not tell in what order the pulse spacings occur. For this we need to look at the text listing of the measured pulse spacings for a clean run of these eight values, such as the one shown in Table 2. From this list of spacings we can see that the order is 3028.03, 2830.25, 3126.85, 2632.50, 3324.62, 2533.65, 3225.75, and 2731.33 microseconds. These values can be expressed as offsets from the average pulse arrival times with spacings of 2929.122 microseconds after rotation of the sequence so that all offsets are positive. The offset values are: 0.00, 395.50, 0.03, 296.65, 98.86, 197.77, 98.90, and 296.63 microseconds. This same sequence

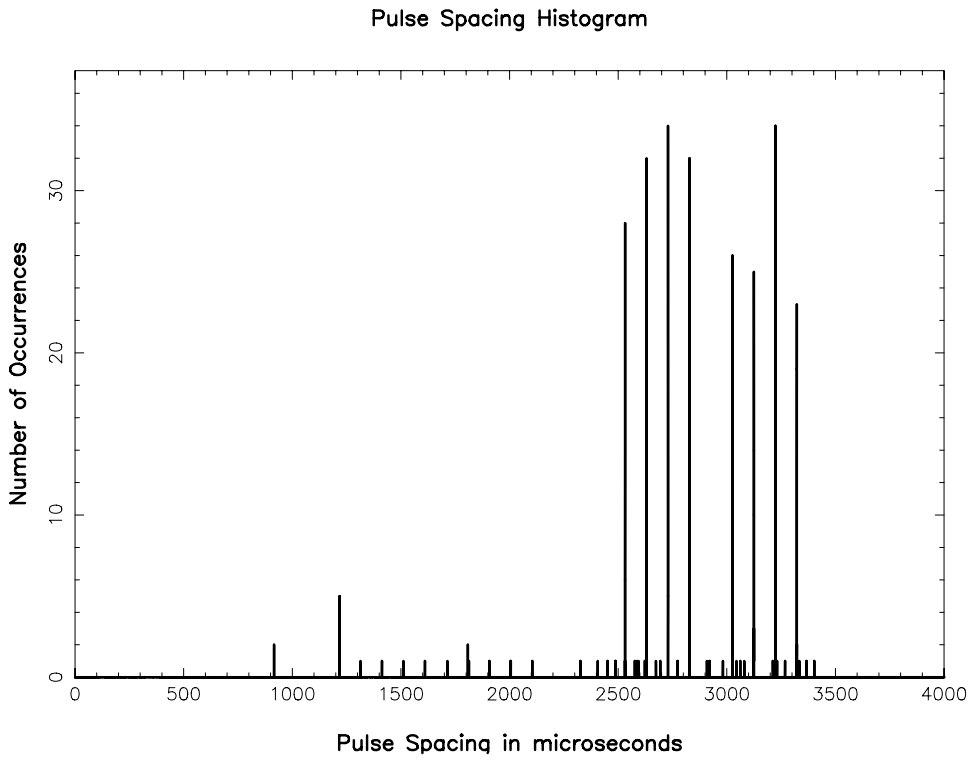

Figure 6: Distribution of spacings between detected first-arrival pulses in about six seconds of data that included a pass of the radar beam over Green Bank. This is from file t33.dat recorded on March 26, 2002.

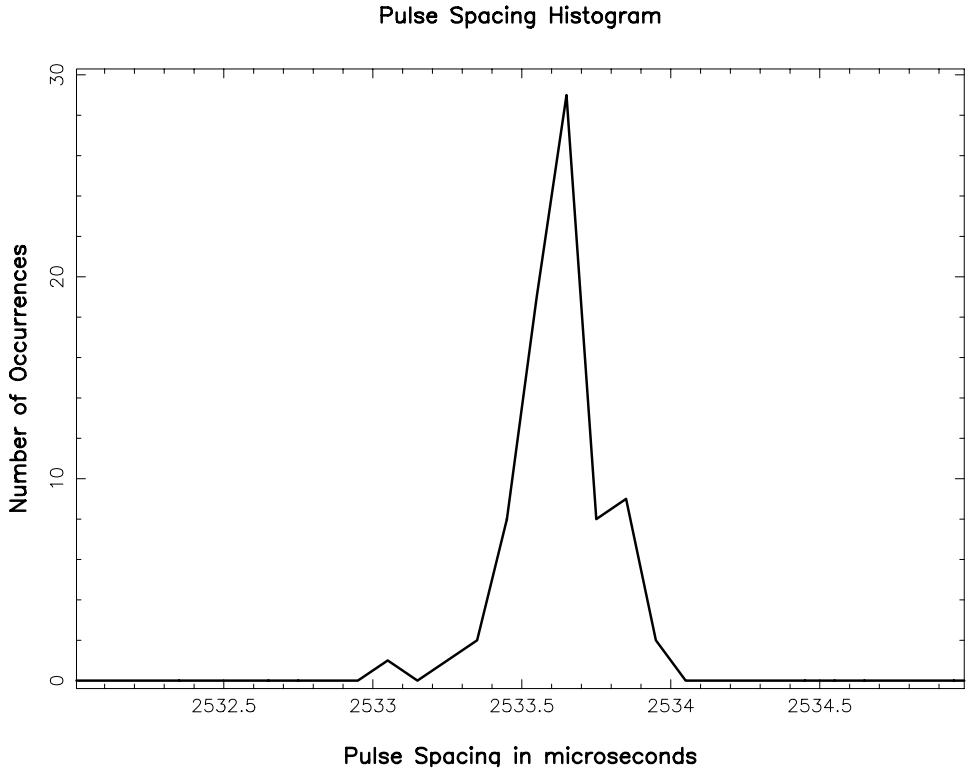

Figure 7: Expansion of plot around the first major peak shown in Figure 6

Table 2: Run of measured pulse spacings in microseconds.

3027.91528320
2830.24536133
3126.89794922
2632.46875000
3324.64672852
2533.53417969
3225.79003906
2731.43115234
3027.80053711
2830.32446289
3126.87622070

was maintained by the radar throughout the 26-month span of measurements listed in Table 1. The two remaining parameters required for data analysis are the time with respect to the beginning of each data set of the first pulse in the sequence listed above and the time of passage of the radar beam over the receiver in Green Bank. The radar beam peak time was estimated by simple inspection of the data as will be seen in the next section. The radar antenna sweep period was measured to be 11.93 seconds from the data sets that spanned 3 minutes (15 rotation periods).

Finding the time of the start of the eight-pulse sequence with respect to the beginning of each data set required finding a solid match between the known pulse spacings listed above and the times of eight successive pulses found in the data set. In most cases the first part of a data set did not contain pulses of sufficient intensity for a good match so successive spans of data were tried until a good match was found. Within one data span the pulse arrival times were measured with the same algorithm described above for determining pulse spacings. Each data span was long enough to contain at least 16 pulses so that a continuous run of the 8-pulse sequence was guaranteed to be contained within the span. When a set of 16 pulses was found the 8-pulse timing sequence was compared with the first eight pulse times, then with pulse times 2-9, the 3-10, etc. At each step the sum of the differences and the sum of the absolute-values differences between the measured and best-fit expected times were computed. If the sum of the differences of one of the comparisons was less than one microsecond, than a match was declared and the offset of the first pulse from the beginning of the data set, modulo the length of the 8-pulse sequence, was computed and saved for further processing of this data set. In most cases the average absolute difference and the average signed difference were less than 0.2 microseconds when the first match was found, and the accuracy of the first pulse time is expected to be roughly the same. There was a slight chance that the match would be found on a set of pulse echoes, rather than the direct-path pulse, but this error would become clearly evident in later data processing.

After the radar pulse timing parameters were determined the pulses could be aligned and there intensity plotted as a function of delay from the direct pulse arrival and of time or radar antenna azimuth as shown in Figure 8. The stripe near the bottom of this figure is from the directly-arriving pulse from the radar. It shows an obvious tilt to negative delays at the right side of the picture, which means that the assumed average pulse repetition rate was too slow. Closer inspection and measurement shows this error to be -11.9 microseconds in 5.8 seconds so the repetition rate was corrected from 341.39917 to 341.39987 pulses per second. The final pulse repetition rate for every data set was checked and, if necessary, corrected in this way.

Figure 9 shows that the radar transmitter's pulse rate clock drifted periodically by a few parts in 10^8 with a period of about 30 minutes. This is what one might expect from a quartz crystal oscillator in a temperature-controlled oven.

6 Reflections from Local Terrain

Figure 10 shows the data in Figure 8 with all timing corrections applied. In this figure a number of significant features are evident. First, the radar beam passed over Green Bank at about 3.09 seconds into the data

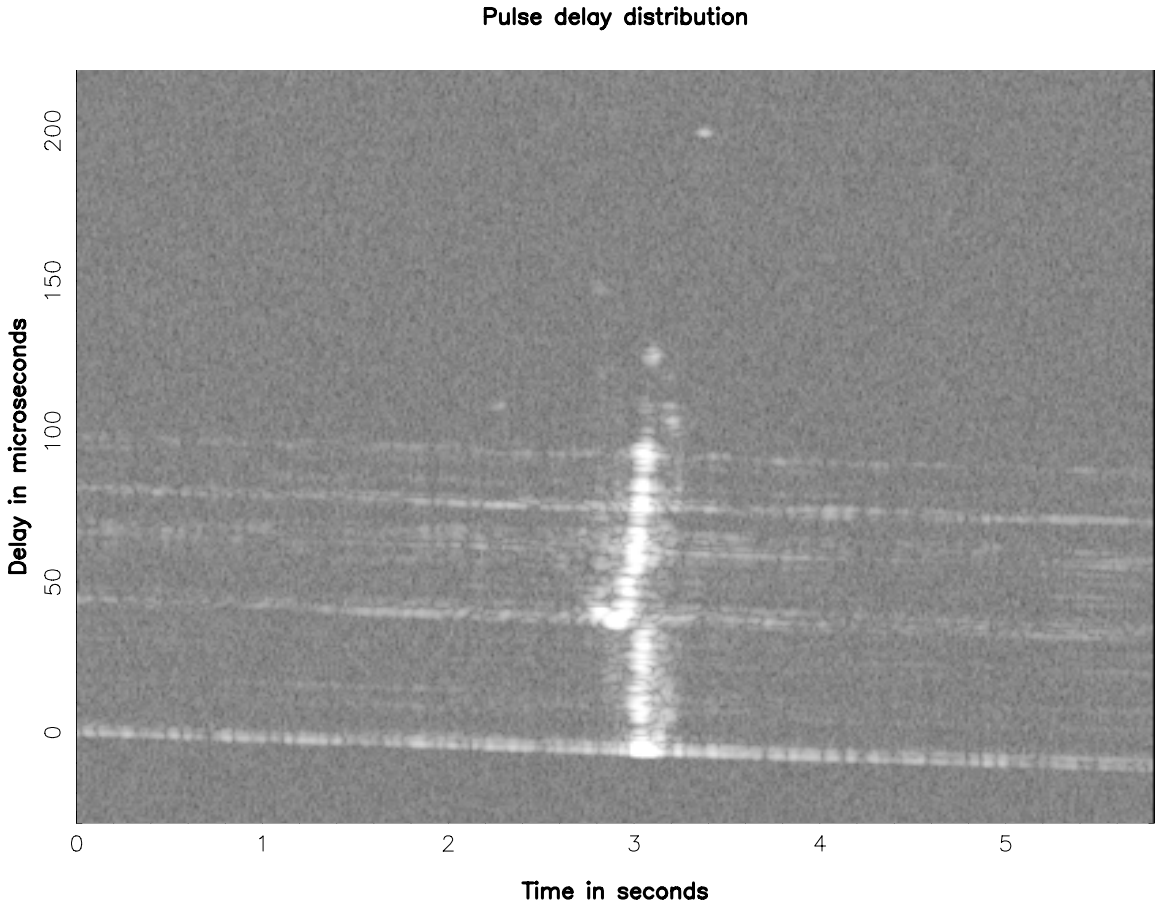

Figure 8: Gray-scale intensity of received pulses. Each vertical row of pixels represents one transmitted pulse interval aligned so that the pulse received directly from the radar falls at zero delay. The horizontal scale is clock time centered roughly around the passage of the radar beam over the receiver near 3.1 seconds. The 5.8 second time span corresponds to an azimuth sweep range of about 175 degrees. An error in the assumed pulse repetition rate is apparent from the droop of the zero-delay stripe. These data were recorded on March 26, 2002 with the sectorial horn pointed to an azimuth of 347 degrees.

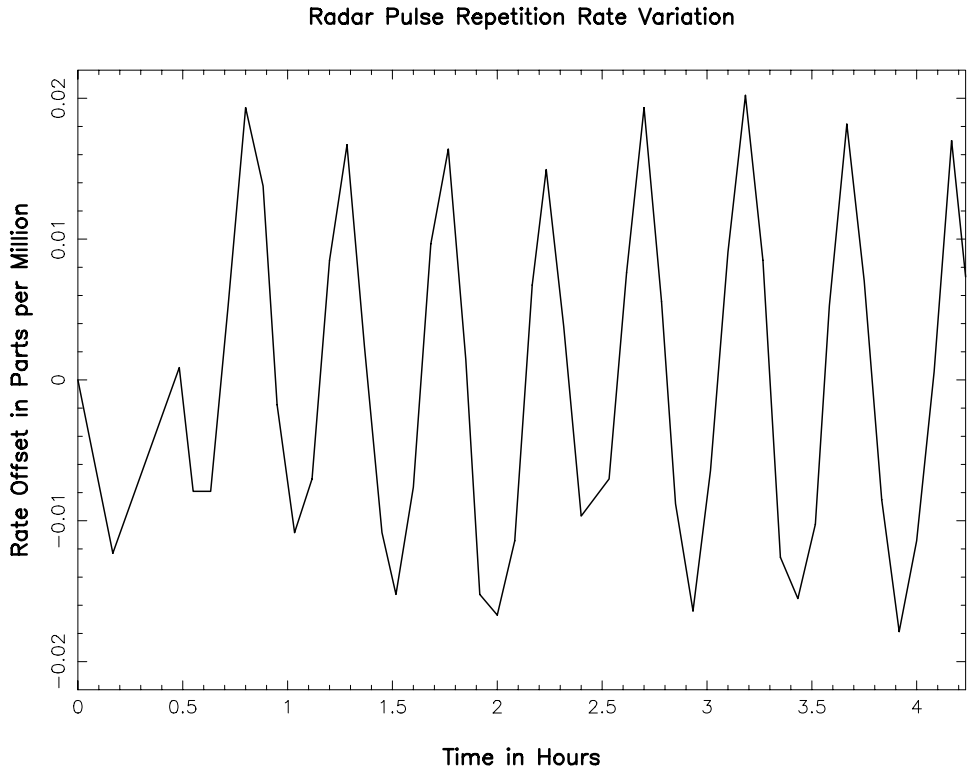

Figure 9: Measured pulse repetition rate difference for each of the data sets in the April 1, 2003 set of observations.

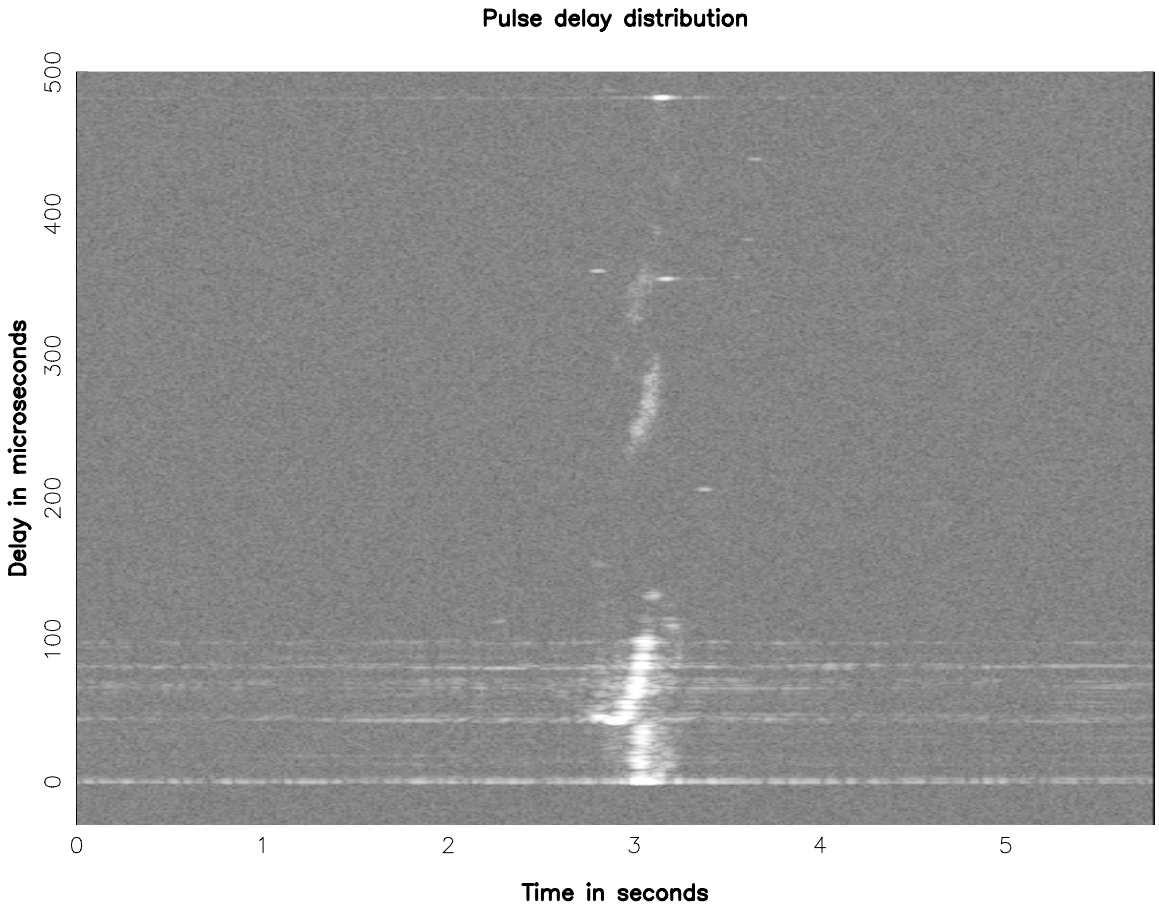

Figure 10: This is the same data as shown in Figure 8 with all timing corrections applied and the delay scale extended to 500 microseconds.

set as measured from the center of the strongest group of pulses at zero delay. Second, the dense clusters of pulse echoes near 3 seconds out to delays of 120 microseconds are due to reflections from local terrain, as will be shown below. Third, the small, isolated echoes between delays of 180 and 500 microseconds are from passing aircraft. Fourth, the wispy features near 3 seconds between delays of 200 and 400 microseconds are reflections from rain cells. Finally, pulses are detectable over all of the measured radar beam sweep, particularly near delays of 0, 45, 67, 82, and 98 microseconds. The weaker pulses in these horizontal features are due to pulses from radar antenna sidelobes reflected by local terrain at the point where the pulses are strongest at that delay.

The delay vs time matrix of pulses can be mapped onto horizontal geographic coordinates by assuming that the pulse reflection points are at the intersections of three surfaces: the constant delay ellipsoid with the receiver and transmitter at the two focii,

$$\frac{x^2}{a^2} + \frac{y^2}{b^2} + \frac{z^2}{b^2} = 1 \tag{1}$$

the vertical plane of the radar beam,

$$\frac{y}{x + \frac{D}{2}} = tan(\theta) \tag{2}$$

and a horizontal plane at a chosen height above the line between the receiver and transmitter.

$$z = Z_0 \tag{3}$$

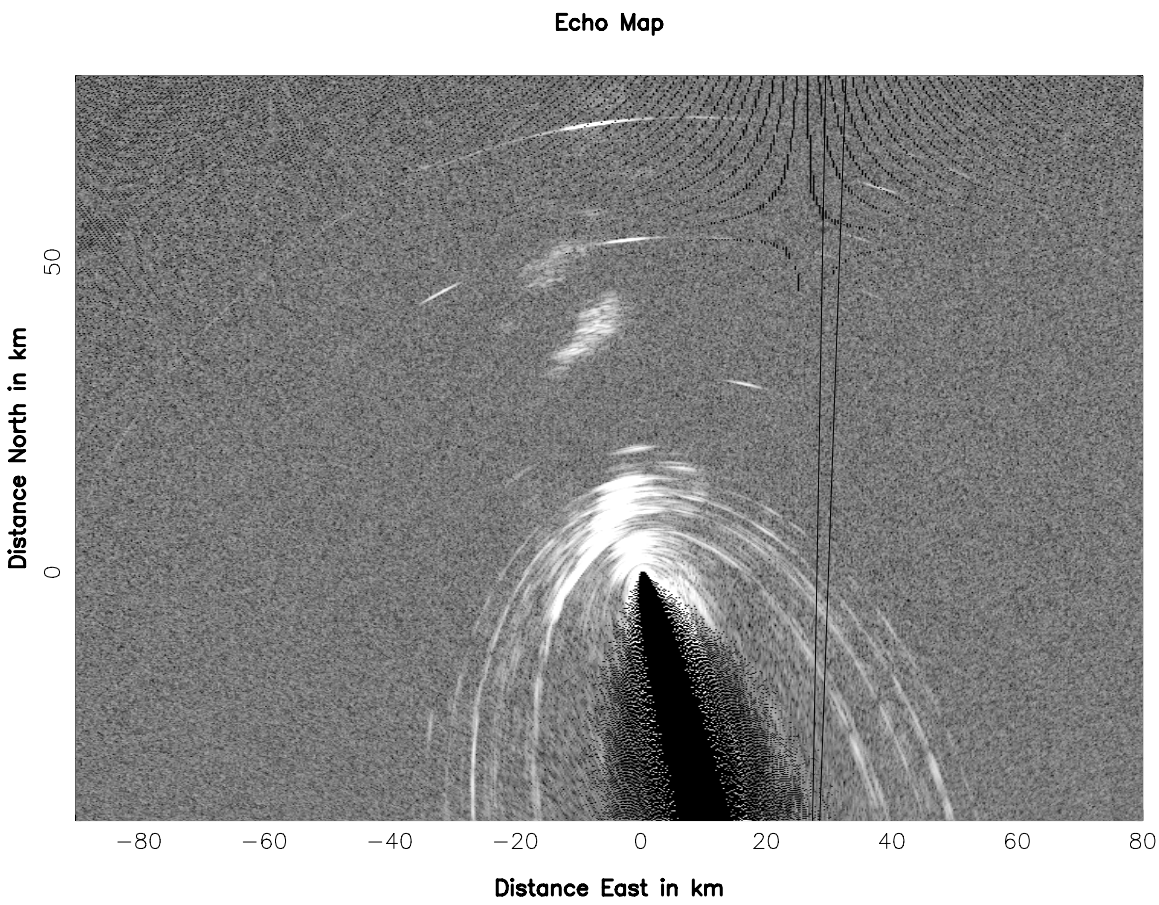

Figure 11: Map of the data in Figure 10 onto horizontal geographic coordinates as explained in the text. The hyperbolic features near the top of the picture are artifacts of the mapping process. The receiver at Green Bank is at the coordinate (0,0) at the upper focus of the ellipses. The radar is at the lower focus off the bottom of the figure. The vertical wedge shows the half-power beamwidth of the radar antenna that sweeps clockwise. The receiving antenna was the sectoral horn pointed to an azimuth of 347 degrees. These data were recorded on March 25, 2002.

Equations 1-3 assume that the transmitter and receiver are on the x axis with the origin at the center of the ellipse so coordinate solutions need to be rotated to the azimuth of the receiver as seen from the transmitter. Locations of reflections not too far above or below the horizontal plane will have significant error in their map projections only when they are close to the receiver or transmitter.

Ellipse coefficients a and b depend on the pulse delay, δt, and the distance, D between the receiver and transmitter,

$$a = \frac{D}{2} + \frac{3 \times 10^5 \delta t}{2} \tag{4}$$

$$b = \sqrt{a^2 - \left(\frac{D}{2}\right)^2}, \tag{5}$$

where δt is in seconds, and d is in kilometers

Figure 11 shows the data in Figure 10 mapped onto the horizontal plane. In this and all maps to follow Z_0 is assumed to be zero. Note that stripes at constant delay in Figure 10 become ellipses in Figure 11.

Figure12 shows a zoom into the region around Green Bank with contours of local terrain elevation above 1200 meters AMSL overplotted. The pulse echoes to the northwest are almost certainly coming from the

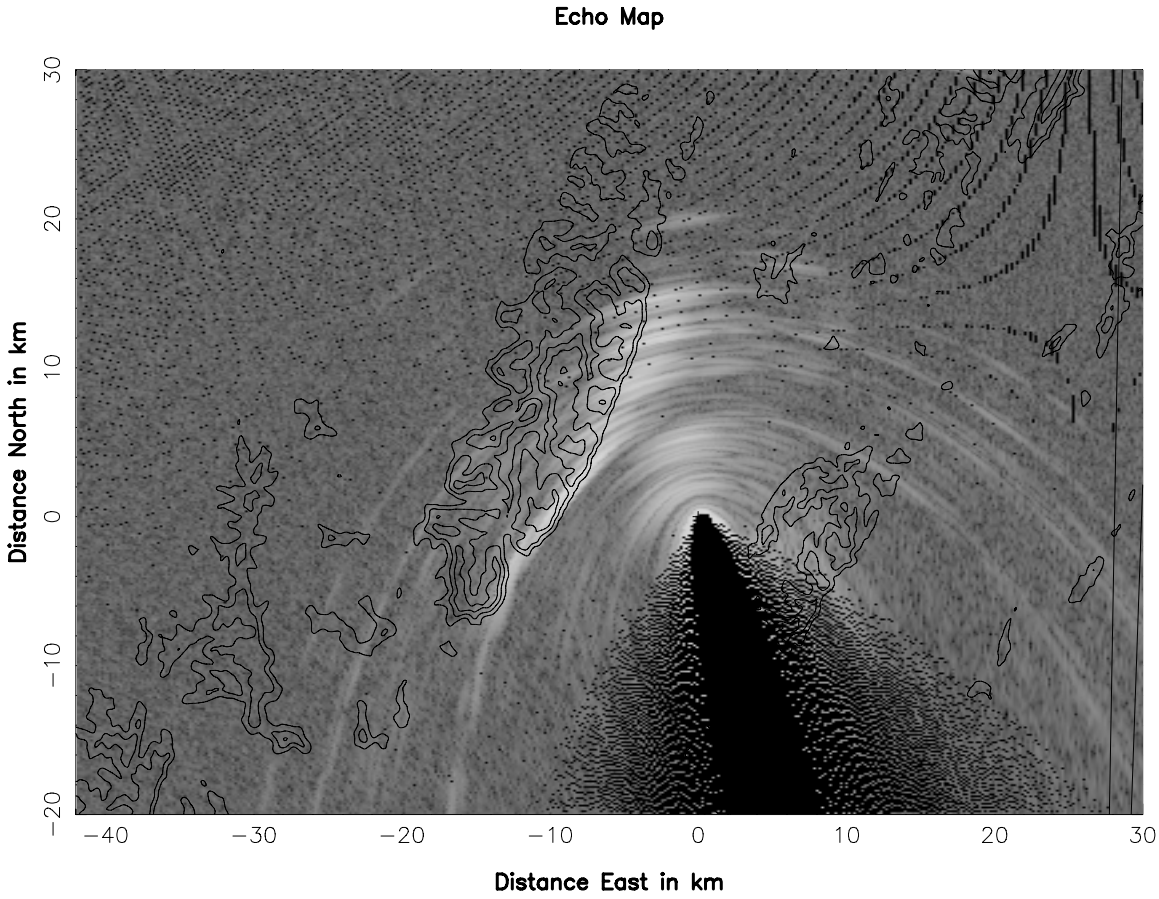

Figure 12: An expansion of the center portion of Figure 11 at lower gray-scale gain to show more detail of pulse echoes around Green Bank. The overplotted contours show terrain elevation at 1200 meters and greater above mean sea level at intervals of 100 meters.

high mountain ridge in that direction that includes the second highest peak in West Virginia, Bald Knob, about 15 kilometers west-southwest of Green Bank.

To verify the location of the radar pulse reflections derived from the pulse delays and radar beam azimuths in Figure 12 the sectoral horn was pointed to two azimuths toward the mountain ridge in the northwest direction and toward the radar antenna to the south-southeast. The results are shown in Figures 13 and 14. These two measurements used 30 dB less gain in the RF amplifier stages to produce a linear response to the strongest received pulses. This test shows that the reflection locations interpreted from delay and radar beam azimuth are correct.

The difference in intensity of the strongest received direct pulses at zero delay with the sectoral horn pointed toward and away from the radar antenna, as shown in Figures 14 and 13 was 17 dB. The strongest pulses received from the mountain ridge (43 microseconds delay) with the horn pointed in that direction (Figure 13) were 19 dB weaker than the strongest pulses received at zero delay with the horn pointed toward the radar antenna (Figure 14). The highest terrain peak, Bald Knob, was out of the sectoral horn beam in both pointings so a direct measurement of its reflected pulse strength is not available. Its reflection is weakly seen in the 310 degree horn azimuth pointing, and, if the horn's response in the direction of Bald knob was 15 dB down from the horn's peak gain, then the reflections from Bald knob were not significantly stronger than those from other parts of the ridge.

Figure 15 is a plot of the maximum pulse intensities at any delay as a function of radar antenna azimuth relative to Green Bank for the two sectoral horn pointings shown in Figures 13 and 14. The relative maximum pulse intensity seen by an isotropic antenna would be roughly the upper envelope of the two

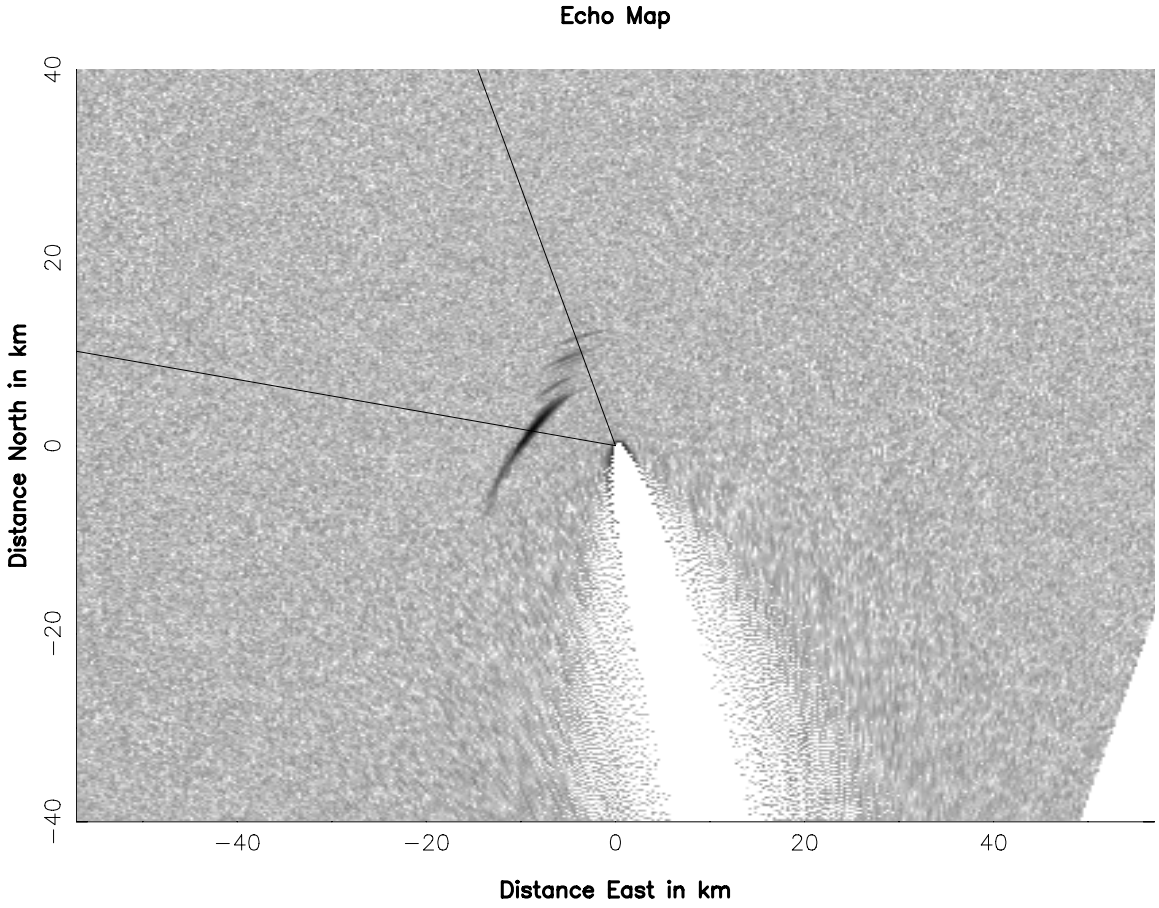

Figure 13: Map of local terrain using 30 dB less gain in the RF amplifier stages than was used for Figures 11and 12 to avoid saturating the receiver with the pulses. The receiving antenna was the sectoral horn pointed to an azimuth of 310 degrees. The 3-dB beamwidth of this horn is shown by the lines drawn from the receiver location. Compare this with Figure 14.

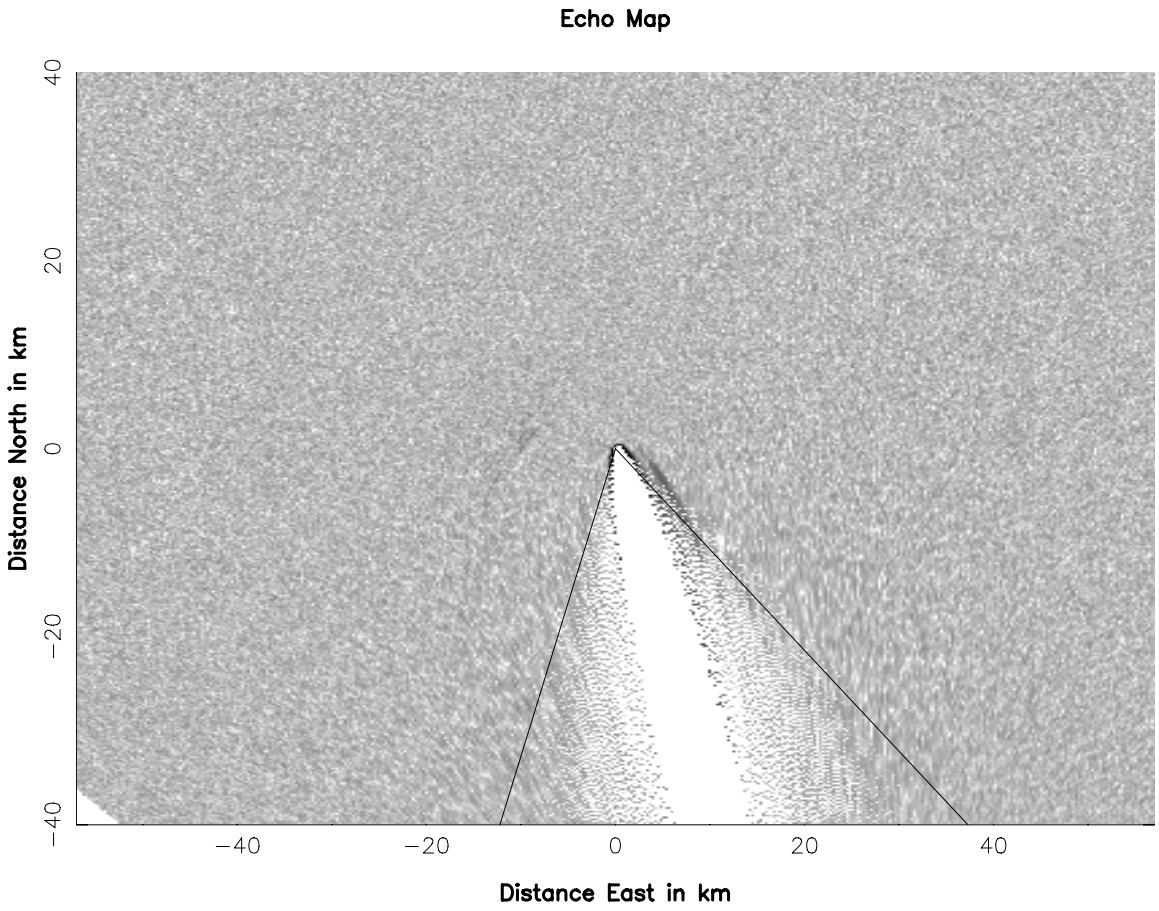

Figure 14: Same plot and receiver gain as used in Figure 13 but with the sectoral horn pointed to an azimuth of 167 degrees as indicated by the 3-dB gain radial lines.

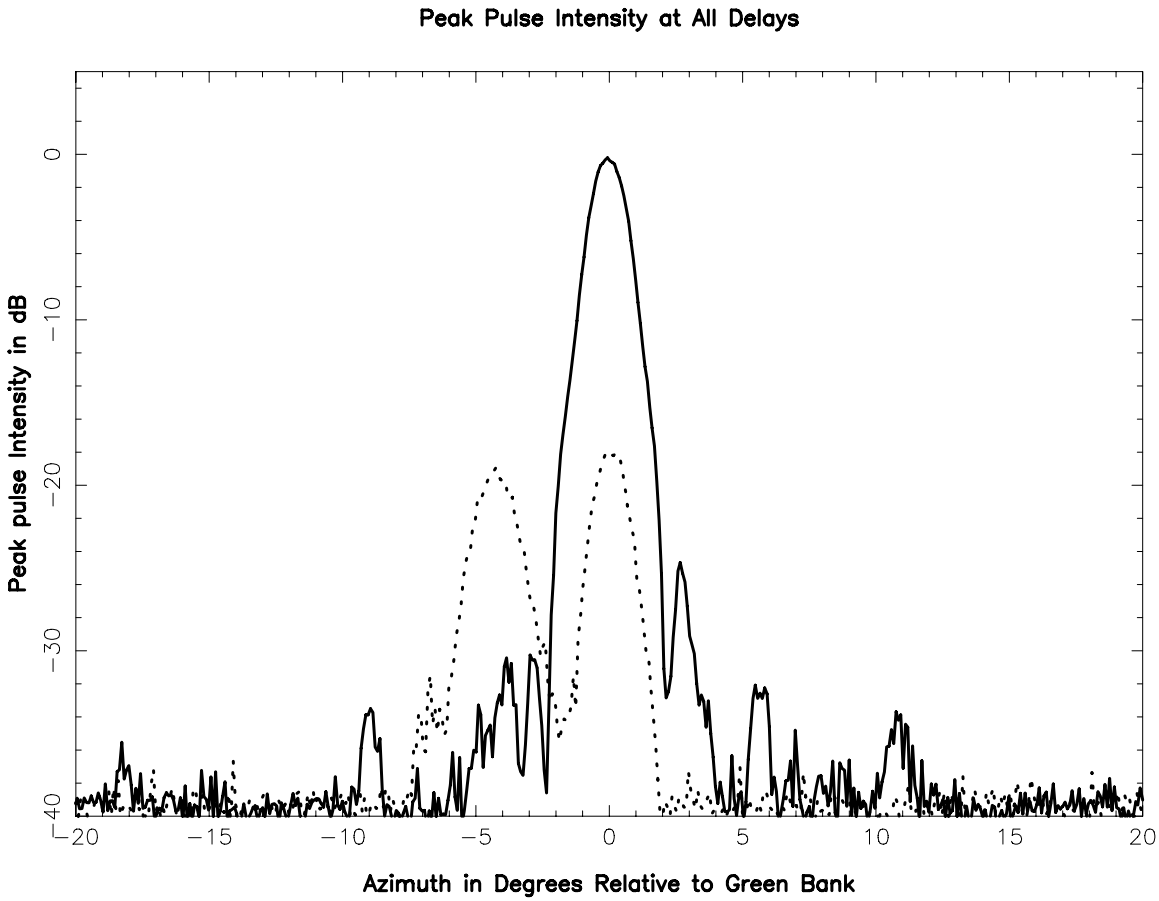

Figure 15: Maximum pulse intensities measured at any delay for the data shown in Figures 13 (dotted curve) and 14 (solid curve).

curves in Figure 15.

The reason that the radar pulses reflected from the mountain ridge are not more than 20 dB weaker than those received directly is shown in Figure 16. The mountain ridge is nearly line-of-site from the radar, particularly when atmospheric refraction in taken into account. Hence, this ridge is well illuminated by the radar. The NRQZ path loss calculation shows that the direct path to the GBT has a diffraction loss of 48 dB from the two highest terrain peaks within 20 kilometers of the GBT. (Diffraction loss to the sectorial horn is unavailable but was likely greater than that to the the GBT focal point.) If we assume that there is no diffraction loss between the radar and the mountain ridge and use the measurement of 19 dB stronger pulses from the direct path, then the scattering loss from the mountain ridge is at least 67 dB. This includes ohmic reflection loss at the scattering point and free space loss between the scattering point and the receiver.

7 Radar Beam Shape

Figure 17 shows the azimuthal pattern of the radar antenna beam plus sidelobes from -55^o to $+32^o$ from the main beam. This plot shows the received pulse power in a narrow delay window of $\pm 1 \mu s$ around the time of arrival of the direct pulse to exclude nearly all echoed pulse power. The 60 dB dynamic range shown in this figure is more than could be obtained with less than 2 microseconds of integration time required for the pulses so the plot is a composite of measurements with four 10-dB steps in RF signal attenuation. Agreement between adjacent 10-dB attenuator values is very good in their common linear response ranges, as can be seen in the overplotted traces. Since the main beam gain is about 35 dBi, all sidelobes more than

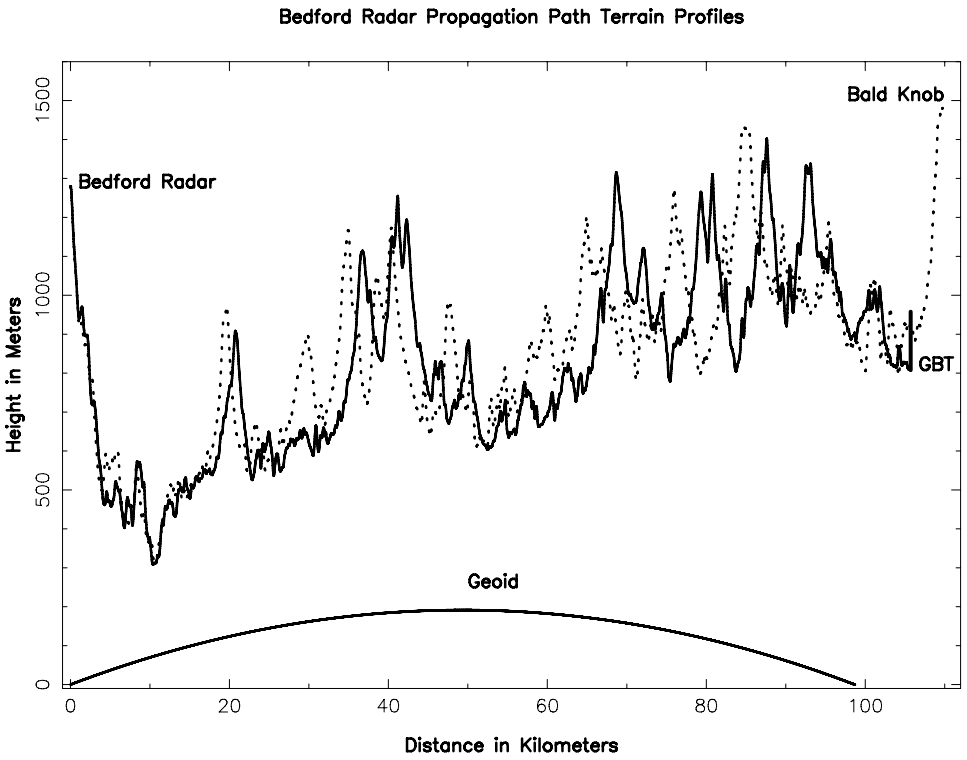

Figure 16: Propagation path profiles from the radar antenna to the GBT (solid line) and to the highest peak on the mountain ridge, Bald Knob (dotted line). The path profile is a vertical cross section of the terrain between the two end points. Note that the vertical scale is 50 times the horizontal scale. The vertical bar labeled "GBT" shows the height of the telescope focal point.

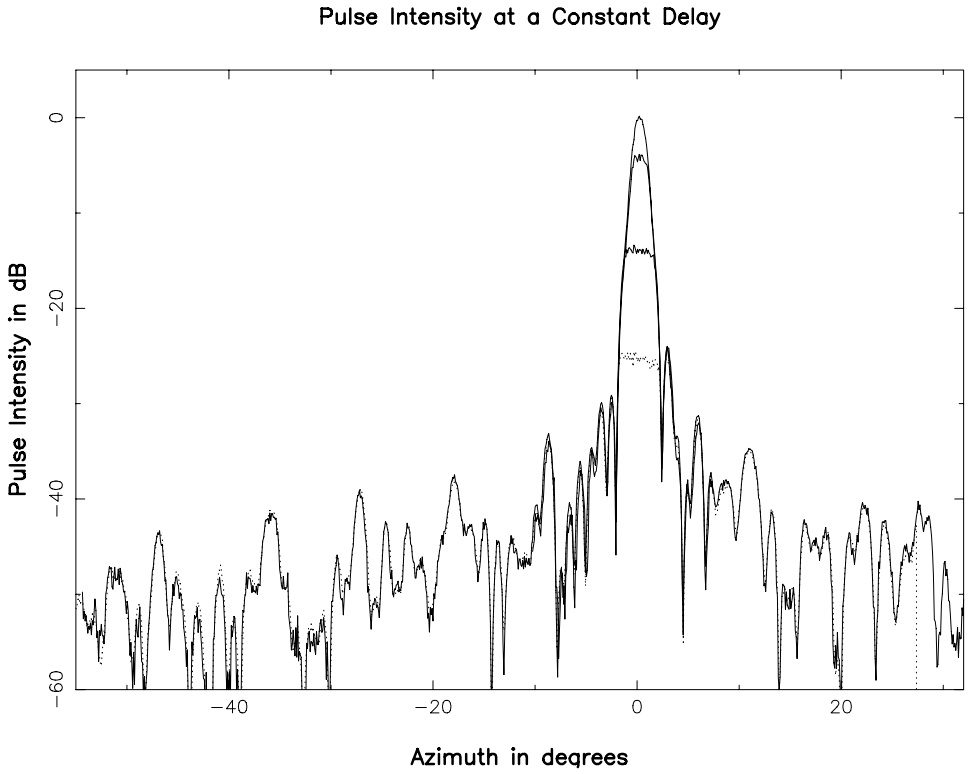

Figure 17: Radar antenna beam pattern and sidelobes. This is a composite plot of zero-delay pulse intensity using four, 10-dB steps of attenuation near the antenna preamp. The sectoral receiving horn was pointed toward the radar antenna. With high attenuation the pulses in the main radar beam were linearly recorded, but the pulses from sidelobes were lost in the noise. (The noisy parts of the plots were suppressed.) With low attenuation the main beam pulses were saturated, but the sidelobe pulses were well above the receiver noise. The minimum attenuation measurement is plotted as a dotted line. Note the good agreement between the two independent traces of weak radar antenna sidelobes (solid and dotted lines).

5^o from the beam center have a gain less than 0 dBi.

The narrow delay window and directional receiving antenna used in measuring the data plotted in Figure 17 will discriminate well against echoes from the terrain behind and to the side of the receiver at Green Bank. However, small-angle scattering from terrain close to the great-circle path between the radar and receiver might not be completely rejected by the delay window. This can be tested by comparing the main beam profile seen in Figure 17 with the received echo beam profile measured on a strong reflection from an aircraft whose pulse delay is well beyond local terrain echoes. The result is plotted in Figure 18. The zero-delay beam is broader by about $\pm 0.4^o$ more than 15 dB below beam peak. If this broadening is due to near-forward scattering from terrain features outside of the vertical plane through the transmitter and receiver, these features would be $\pm$600 meters from this plane, assuming that they are at a distance of 87 km corresponding to the highest peak in Figure 16. The 3-dB beamwidth measured with all curves in Figure 18 is about 1.3 degrees.

8 Rain Shower Reflections

Figures 10 and 11 show fuzzy patches of radar pulse reflections slightly to the west of north of Green Bank at distances between about 30 and 50 kilometers. These patches were seen on eight successive maps spanning a 23-minute interval on the Morning of March 26, 2002. Maps from the last 15 minutes of this sequence are shown in Figure 19. The progression of the rain showers can be seen as cells moved to the

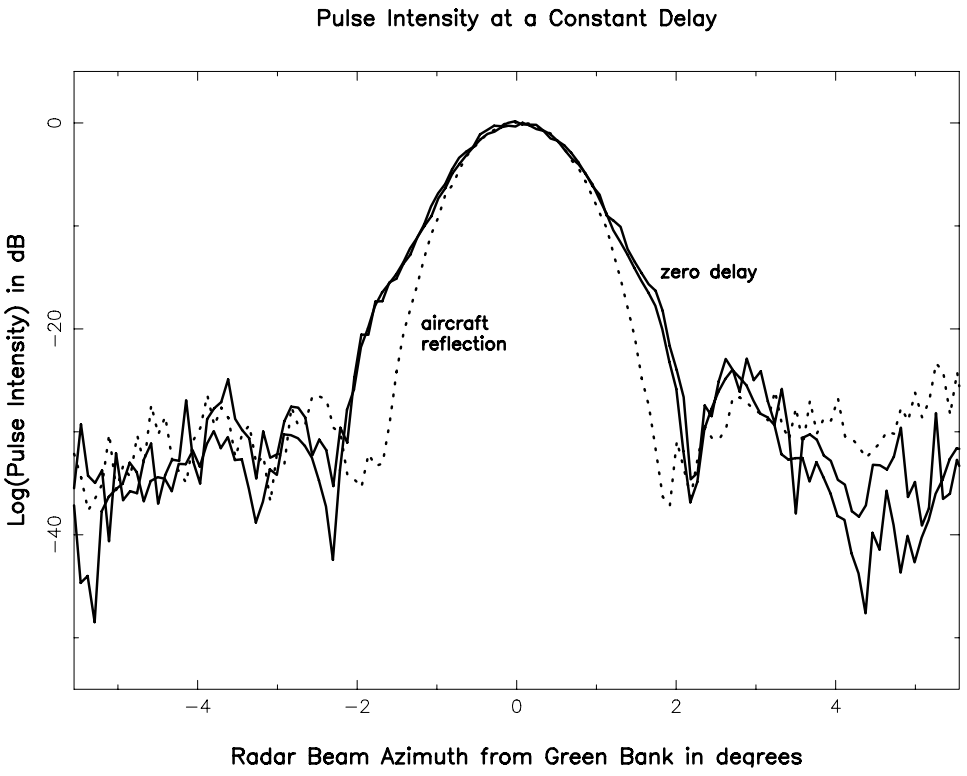

Figure 18: Comparison of azimuthal beam pattern of the radar antenna measured with zero-delay pulse intensities (solid curves) as described in Figure 17 and associated text and with a strong reflection from an aircraft (dotted curve).

northeast and then disappeared. A new cell from which strong radar pulses were detected appears in the second frame near coordinates (x=-23,y=+25) and reached maximum intensity around frame 5. The NEXRAD radar archive (http://www4.ncdc.noaa.gov/cgi-win/wwcgi.dll?WWNEXRAD Images2) for this time and date shows a strong band of rain showers along a southwest to northeast line through Pittsburgh, PA, plus scattered showers through far-southwest Virginia. This band of showers was moving rapidly to the east-northeast. The rain cells shown in Figure 19 were very likely part of the southern edge of this rain band.

9 Comparison of GBT and Sectorial Horn Data

Most of the data shown in previous sections were recorded with the sectorial horn at the RFI monitor station near the works area. The GBT feed is about 120 meters higher above the ground, and its far sidelobes are distributed more or less randomly around the horizon. Hence, we expect the GBT to see a different distribution of terrain echo intensities. This difference is show in Figure 20. The GBT sees a stronger echo from the nearby terrain to the north-northwest as is evident in the bright sidelobe ellipse at a distance of about 10 km. The GBT also sees echoes from more distant terrain to the north and west.

10 Variable Propagation

Radar signal strengths from terrain echoes can be quite variable as illustrated in Figure 21. Over a period of about an hour just before midnight of March 31, 2003 quite a few new echoes gradually appeared on the radar map measured with the GBT in almost all directions. Several small, bright features can be seen at the bottom of the right hand map to the southwest of the radar antenna, and an extended ridge appeared to the southwest of Green Bank to a distance of about 50 km. The most remarkable new features are on the east side of this map at a distance of about 100 km. The brightest spot on the west side of this group of echoes corresponds to the high terrain parallel to the Blue Ridge Parkway just north of Rockfish Gap where Interstate 64 crosses Afton Mountain. More echoes can be seen to the northeast of this location about 12 km further along the Blue Ridge. About 10 km to the east of the Rockfish Gap echo a reflection from Yellow Mountain, to the south of Crozet, VA, can be seen. Yellow Mountain is considerably lower than the Blue Ridge and should be hidden from the Green Bank direction, but this lower ridge must be illuminated strongly enough by the radar that the GBT can see its signal diffracted over the higher ridge. The observing session ended while the distant echoes were clearly visible so we don't know how long these propagation conditions lasted into the early morning of April 1.

11 Aircraft Reflections

On February 2, 2003 a continuous run of data was recorded for ten minutes using the sectoral horn pointed north for the purpose of watching the motion of aircraft echoes. This data run included 50 rotations of the radar antenna, and, hence, 50 reflection maps were plotted. Figure 22 shows the last of these maps where six aircraft reflections are apparent as well as a small rain shower about 30 km to the north-northwest of Green Bank. Figure 23 shows the locations of aircraft reflection on all 50 maps overplotted on the map in Figure 22. Several of the tracks, particularly the one just to the north of Green Bank, include reflections from several different aircraft on that route at different times during the ten minutes. In a time sequence at the location (-5 km, +30 km) two aircraft can be seen turning onto the well-traveled track from an ESE heading to a WSW heading as can be seen by the little crescent shaped trail of circles. The intensity of the reflections from any one aircraft varied considerably from one 12-second sweep of the radar antenna to the next.

12 Reflection Intensities

Since reflections from rain showers and aircraft are received for only a small fraction of the time between radar pulses and only about 0.5% of the radar antenna's sweep period one would like to know whether it is worth the trouble and data loss to blank the GBT receiver for more time than is occupied by direct pulses

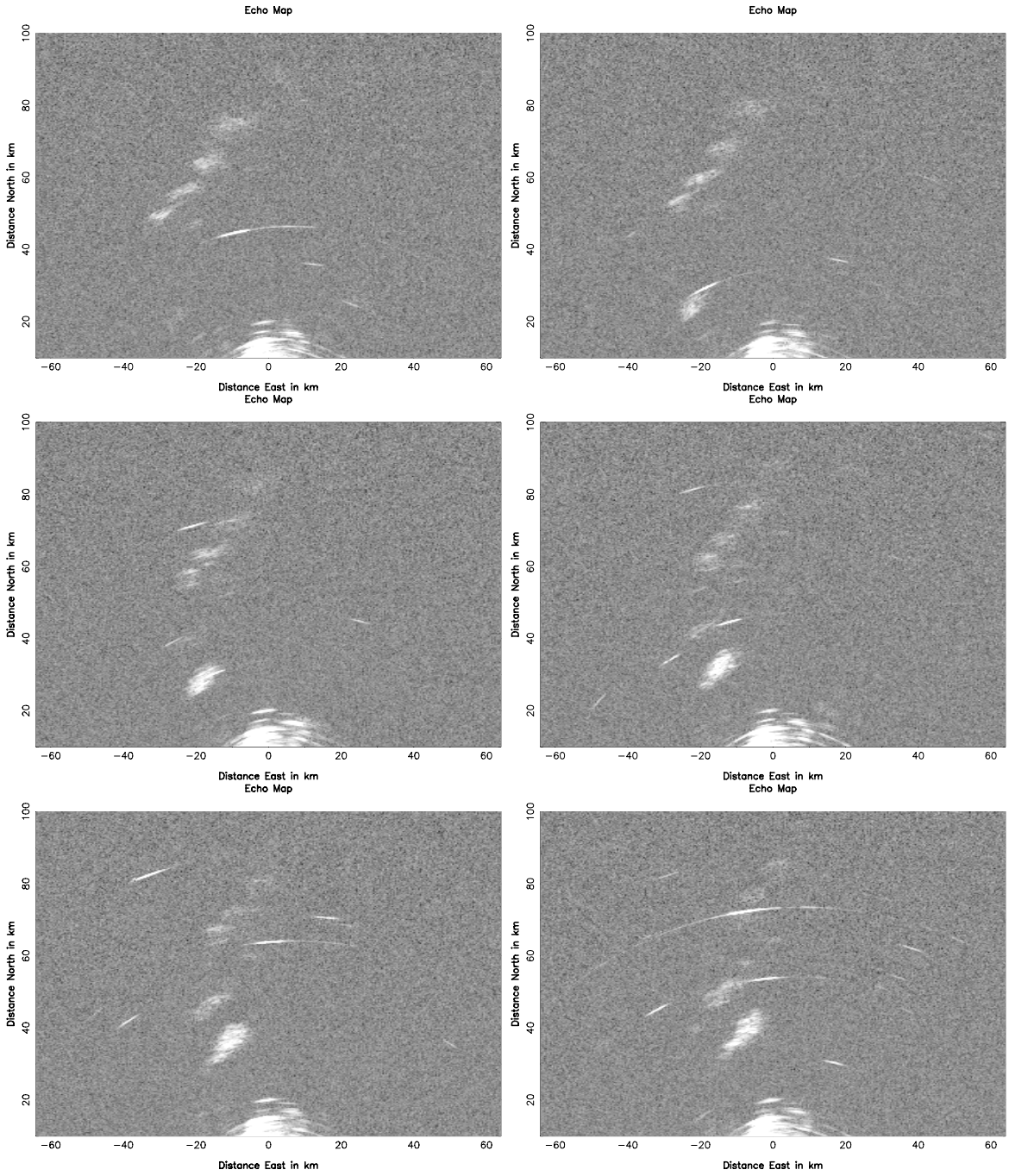

Figure 19: Radar reflection maps at three-minute intervals showing the progression of rain showers to the north of Green Bank between 10:39 and 10:51 EST on March 26, 2002. The time sequence is top left, top right, middle left, etc.

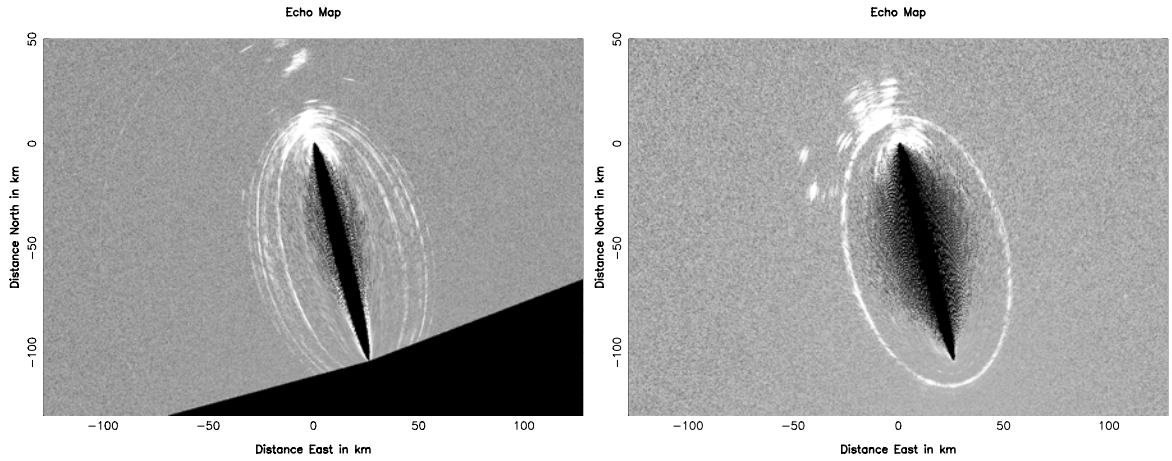

Figure 20: Comparison of terrain reflection distribution seen by the sectorial horn pointed to an azimuth of 347 degrees (left) and by the GBT feed (right). The sectorial horn data is the same as shown in Figures 11 and 12. The GBT data were recorded on April 17, 2003 while observing redshifted hydrogen in the galaxy 1007+0121. The echoes at the top of the sectorial horn map are from rain showers and aircraft.

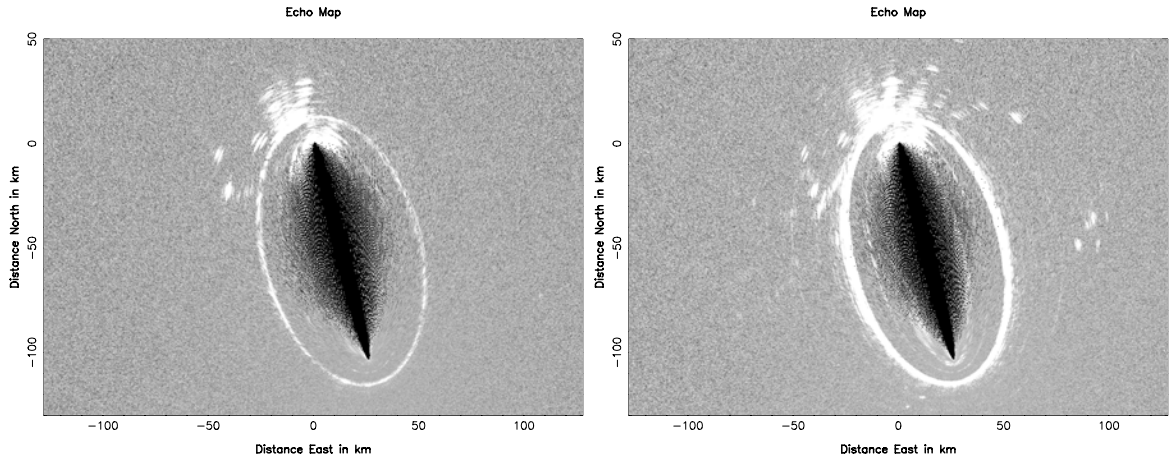

Figure 21: Enhanced propagation conditions. The terrain echo pattern most commonly seen by the GBT is shown on the left. On the right is the echo pattern seen on March 31, 2003 near midnight local time.

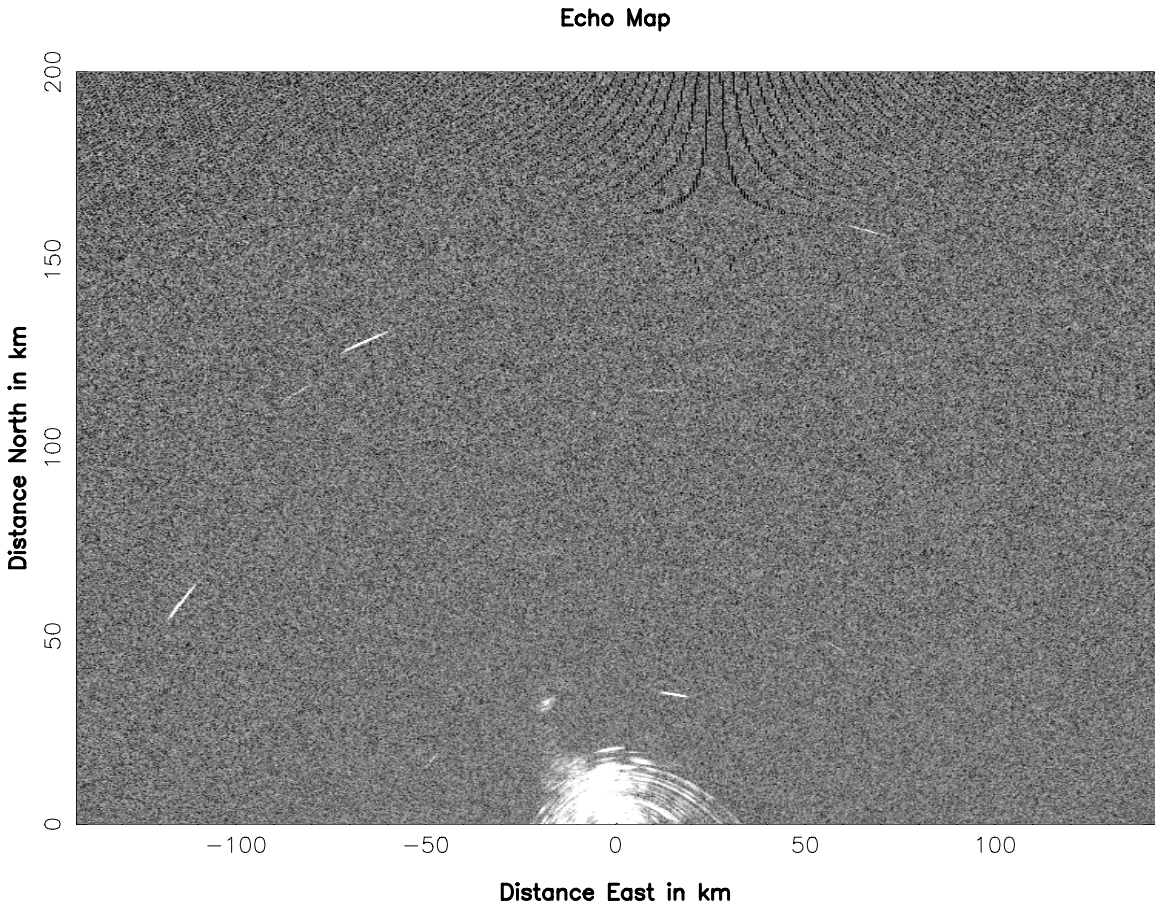

Figure 22: Radar map showing at least five echoes from aircraft seen as short arcs. A small rain cell is also visible at coordinates (-20,30).

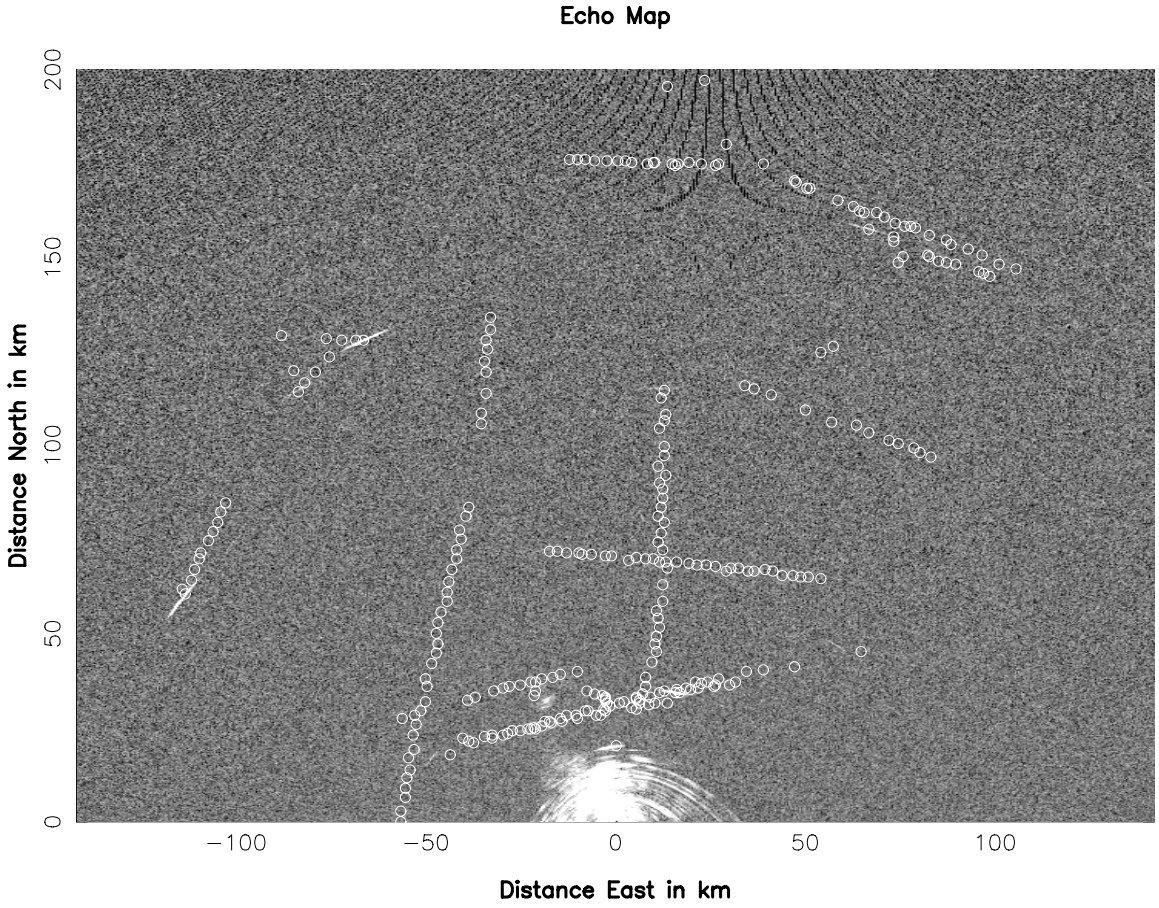

Figure 23: Same map s shown in Figure 22 with echo locations of aircraft seen on 50 successive sweeps of the radar beam overplotted.

Table 3: Ratios of measured pulse intensities to the total system noise in a 0.5 MHz bandwidth for various sources of reflection averaged over the 12-second radar antenna sweep period using the data shown in the bottom left panel of Figure 19.

Reflector	Avg. Intensity
Terrain	1.21938
Sidelobes	0.01044
Rain	0.00309
Airplane 1	0.00014
Airplane 2	0.00275
Airplane 3	0.00026

and reflections from local terrain. A rough answer to this question can be made by measuring the intensity of the various echoes averaged over one radar antenna sweep time of 12 seconds. Table 3 shows the results using the data shown in the bottom left panel of Figure 19. This measurement used a horn antenna with a gain roughly 20 dB higher than the average far-sidelobe gain of the GBT, but the system noise of the measurement receiver was about 14 dB higher than the GBT's receiver so the ratio of pulse reflection to system noise may be a factor of four too pessimistic for GBT observations.

The numbers in Table 3 can be compared to the rms noise in a five-minute observation on the GBT with a 100 kHz bandwidth, which are typical parameters that an astronomer would use in the measurement of neutral hydrogen in a galaxy redshifted to the frequency of the radar. The astronomical measurement would integrate for several hours or more, but the integration would be broken into five-minute-on-source/five-minute-off-source integration pairs, where the on-source spectrum is subtracted from the off-source spectrum. Hence, some cancellation of the radar signal can be expected for time intervals greater than five minutes. The rms noise is

$$\frac{\Delta T}{T_{sys}} = \frac{1}{\sqrt{300 \times 1 \times 10^5}} = 0.000183 \tag{6}$$

Hence, all but the weakest reflections from aircraft seen in Figures 19, 22, and 23 can cause significant errors in a five-minute spectrum integration.

13 Oddities

The observations of redshifted hydrogen radiation from 1007+0121 and UGC4288 with the GBT included radar data from more than 900, 12-second radar antenna sweeps. Radar maps were made of all of these sweeps with corner dimensions of (-326, -260) and (326, 200) kilometers relative to Green Bank in one of the two GBT receiver polarizations. All of these maps were looked at for interesting radar echo features. In addition to the enhanced propagation conditions shown in Section 10, two weak, apparently linear features were seen in successive radar antenna sweeps shown in Figure 24. The features appeared with roughly equal strength in both GBT receiver polarizations. Nothing was evident on previous or subsequent radar sweeps.

Whatever the enhanced radiation was it had to be synchronous with the radar pulse timing over many pulses. These were not ordinary short bursts of wideband interference, because this type of interference produced a radial track that ran through the radar antenna location at the bottom focus of the dark ellipse. Terrain echoes seem unlikely to be the cause of the features in Figure 24 because of the straightness of the features. Ionized meteor trails can reflect microwaves, but these are typically 70 to 110 km above ground [Carbognani *et al (2001)*], and the second track came within about 30 km of the radar antenna using the geometrical assumptions that went into these maps. Also, 1200 MHz is an unusually high frequency for meteor track reflections. The variable pulse spacing would tend to argue against some sort of aliasing effect, but this is a possibility. These features remain an intriguing mystery.

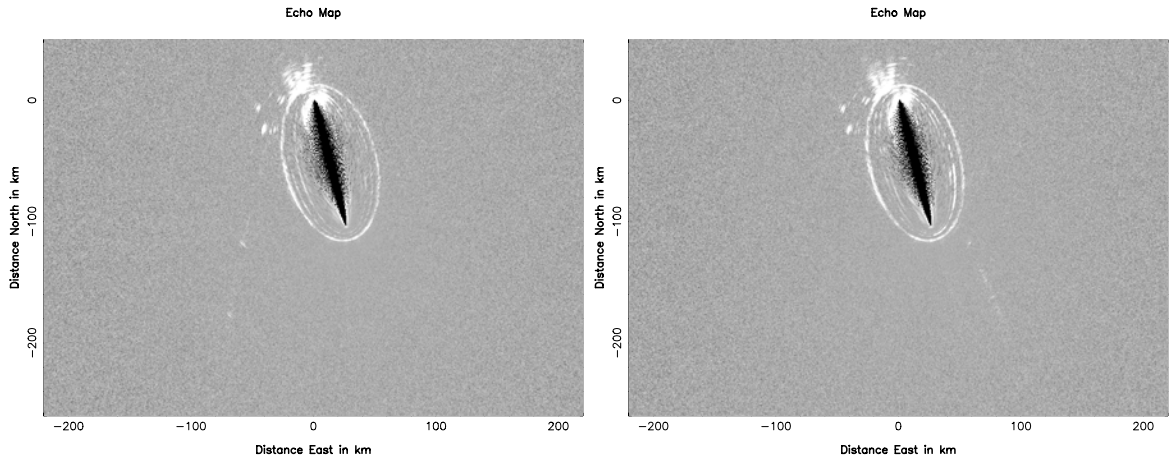

Figure 24: Curious linear features in two successive radar antenna sweeps seen in GBT data on April 17, 2003. In the left map the feature runs from about (-80, -180) to (-50, -100) with two prominent knots. In the right hand map the line runs from about (+100,-200) to (+60, -110).

14 Integrated Spectra with Blanking

On March 31 and April 1, 2003 120 minutes of GBT integration time was devoted to measuring the HI line profile of the galaxy UGC 4288 (B1950 ra = 08h 11.7m, dec = +19d 30m). The redshift of this galaxy puts the low-frequency edge of its line profile within about 1 MHz of the FAA radar frequency. Hence, we can test the efficacy of blanking the radar pulses from the same spectral data that contains a weak astronomical signal.

The observing was divided into 3-minute integrations with the telescope pointed alternately at UGC 4288 and at a region of blank sky 5 minutes of right ascension to the east. Two orthogonal, linearly polarized receiver channels were recorded. Each receiver bandwidth was 5 MHz centered on 1290.69 MHz with its baseband signal sampled at 10 MS/s. The offset of the radar pulse sequence from the beginning of a 3-minute data set and the pulse repetition rate were determined independently for each data set as described in Section 5. These parameters were used to blank data at selected intervals relative to each pulse's direct-path arrival time.

Spectra were generated by Fourier transforming groups of 2048 data points to create 1024 spectral channels of 5 kHz spacing. When a 2048-point data group extended into a blanking window the data group interval was backed up in time to abut the beginning of the blanking window (causing some overlap with the previous group), and the next 2048-point group began at the end of the blanking window. Each 1024-channel complex spectrum was squared and added to the spectrum accumulator. At the end of the 3-minute integration the spectral power values in this accumulator were normalized by the number of spectra accumulated. The resulting sum of (on - off) / off spectra, using radar pulse blanking 5 μs before to 120 μs after the direct-arrival pulse time, are shown in Figure 25. Figure 26 shows the same spectra as in Figure 25 but without radar pulse blanking. A blanking window of -5 to +120 μs relative to the direct-arrival pulse times appears to be quite effective in removing the radar signal from the astronomical data

The hydrogen line profile of UGC 4288 shown in Figure 25 has a 20% peak intensity line width of about 518 km/s, a systemic velocity of 30212 km/s, and an integrated line intensity of 2.16 Jy km/s. These values agree reasonably well with values of 558 km/s, 30223 km/s, and 2.54 Jy km/s, respectively, measured at Arecibo by [O'Neil *et al (2004)*].

The intensities of radar echoes listed in Table 3, Section 12 from aircraft with delays greater than 120 μs suggest that there may be some weak radar signal residual in the spectra of Figure 25. A sensitive test for radar signal residual can be made by generating total power spectra with different blanking window lengths using all data integrated over the 120 minutes of observing. Figure 27 shows the (spec1 - spec2) / spec2 results, where spec2 is the spectrum using a blanking window from -5 to +999 μs, and spec1 is the spectrum from the same data with progressively shorter blanking windows, all starting at -5 μs. Some radar signal

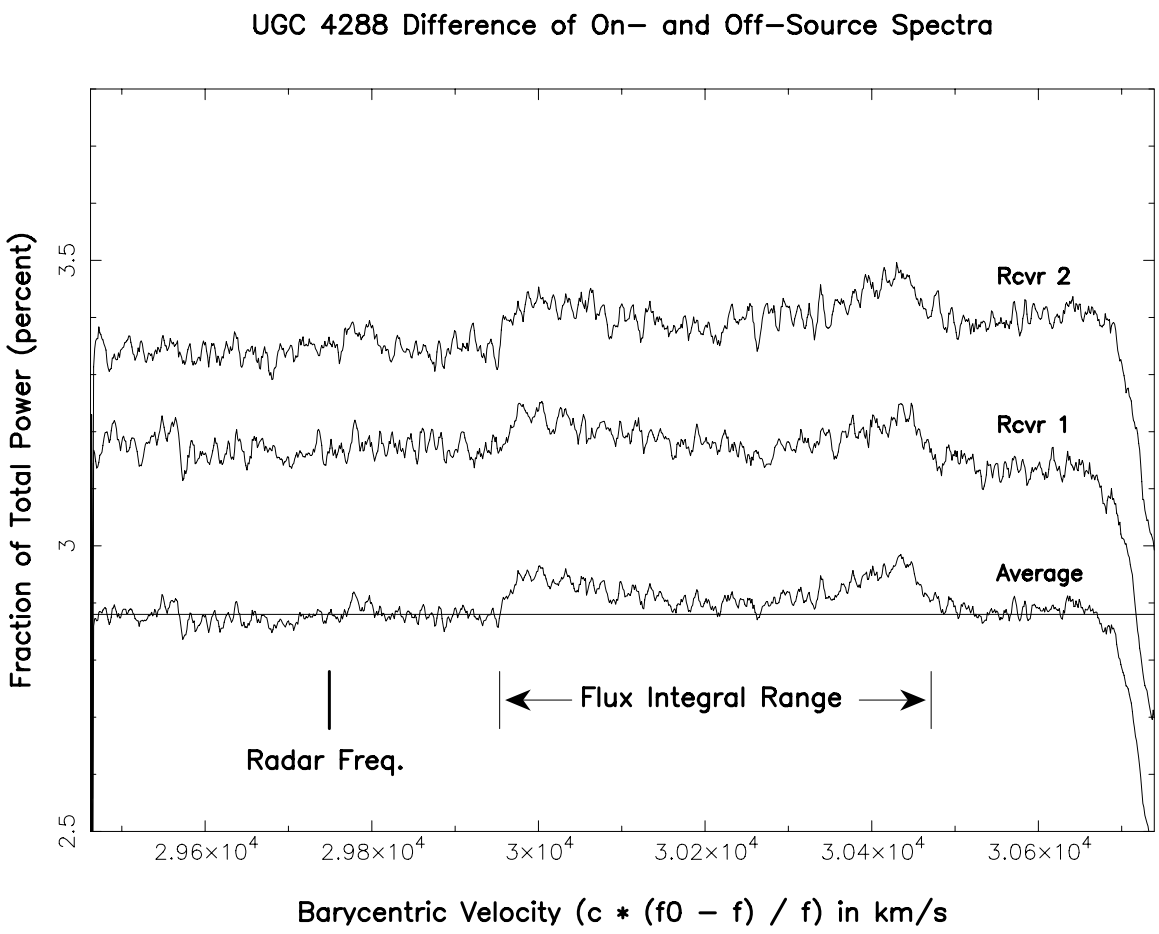

Figure 25: Integrated spectrum of UGC 4288 using 48 minutes of integration (24 on-source and 24 off-source) from March 31 and 62 minutes from April 1. The blanking window was from 5 μs before the direct pulse arrival time to 120 μs after. The conversion from measured frequency to velocity used the "optical definition" of $c(f_0 - f)/f$, where c is the velocity of light, f_0 is the HI rest frequency, and f is the measured frequency of each spectral channel. The vertical scale is normalized to the total system power, where $1\% \approx 0.23\ Kelvin \approx 0.1\ Jy$. The spectra were convolved with a 5-channel rectangular function to a resolution of 25 kHz (5.8 km/s).

can be seen in spectra with blanking of 300 μs and less. Note that the noise in these spectra is less than the rms of 0.033% that one might expect from 120 minutes of integration because the same data are used for spec1 and spec2 except for the data blanked by the longer window but not the shorter.

The residual intensity with a blanking cutoff of 120 μs at the peak of the radar signal in Figure 27 is 0.048% of system noise power. With no blanking in these data the radar peak intensity is 32% of system noise power. The sweep-averaged intensities of aircraft echoes listed in Table 3 range from 0.0035 to 0.069% (after adjusting or the factor of 4 difference in gain and system temperature of the horn antenna and GBT), which are consistent with the residuals seen in Figure 27. Because the residual radar signal is present in both "on" and "off" spectra used in Figure 25 there will be some additional cancellation in the difference. Figure 28 shows the (on - off) / off spectra for UGC 4288 using blanking widow cutoffs of 120 and 500 μs plus an expanded-scale difference of these two spectra. At the radar frequency the spectral power difference is about 0.006% of system noise power. Hence, the (on - off) differencing process for 20 "on" and 20 "off" spectra suppressed the radar signal by about a factor of 8. Again, note that the rms noise in the difference spectrum at the bottom of Figure 28 is less than the rms noise in either of the two spectra above it because the same data set was used in the two spectra.

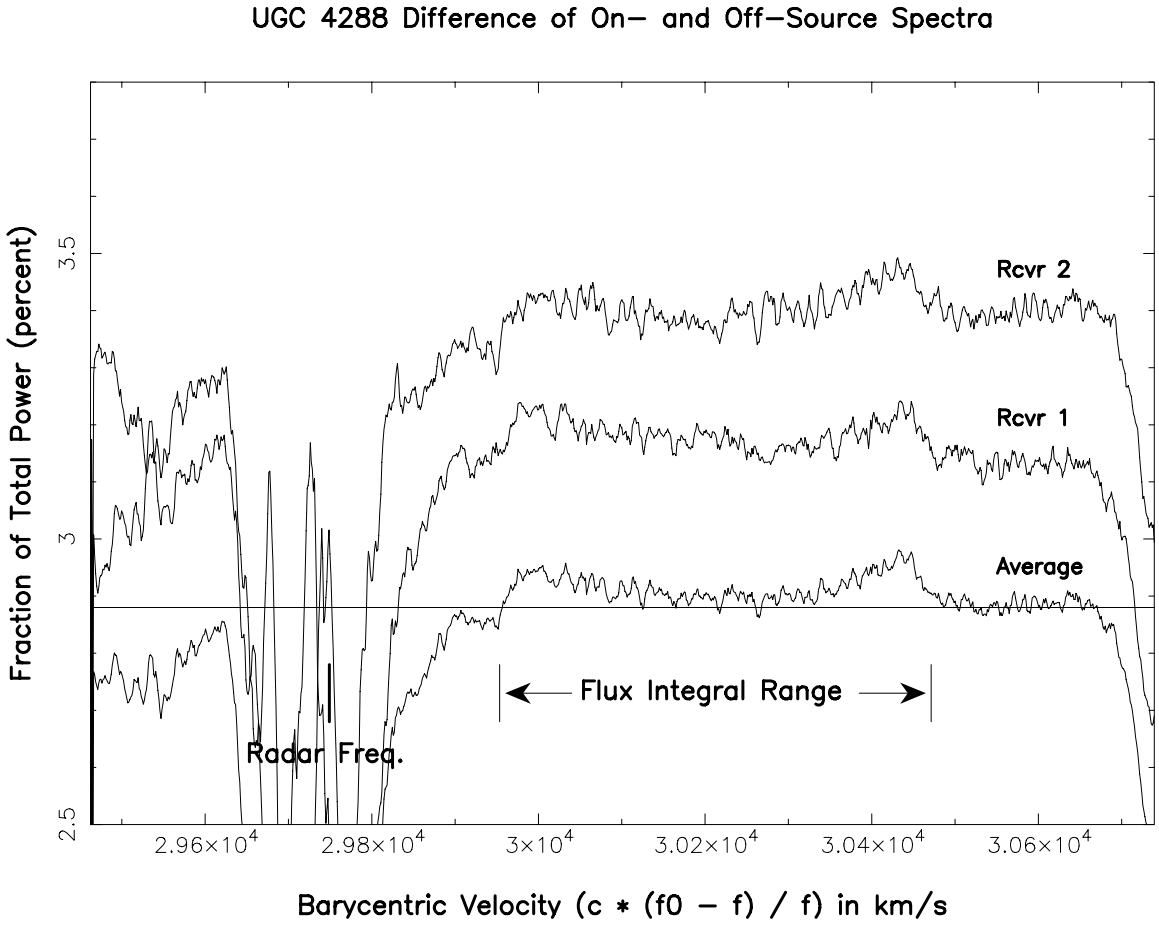

Figure 26: Same data and analysis as in Figure 25 but without radar blanking

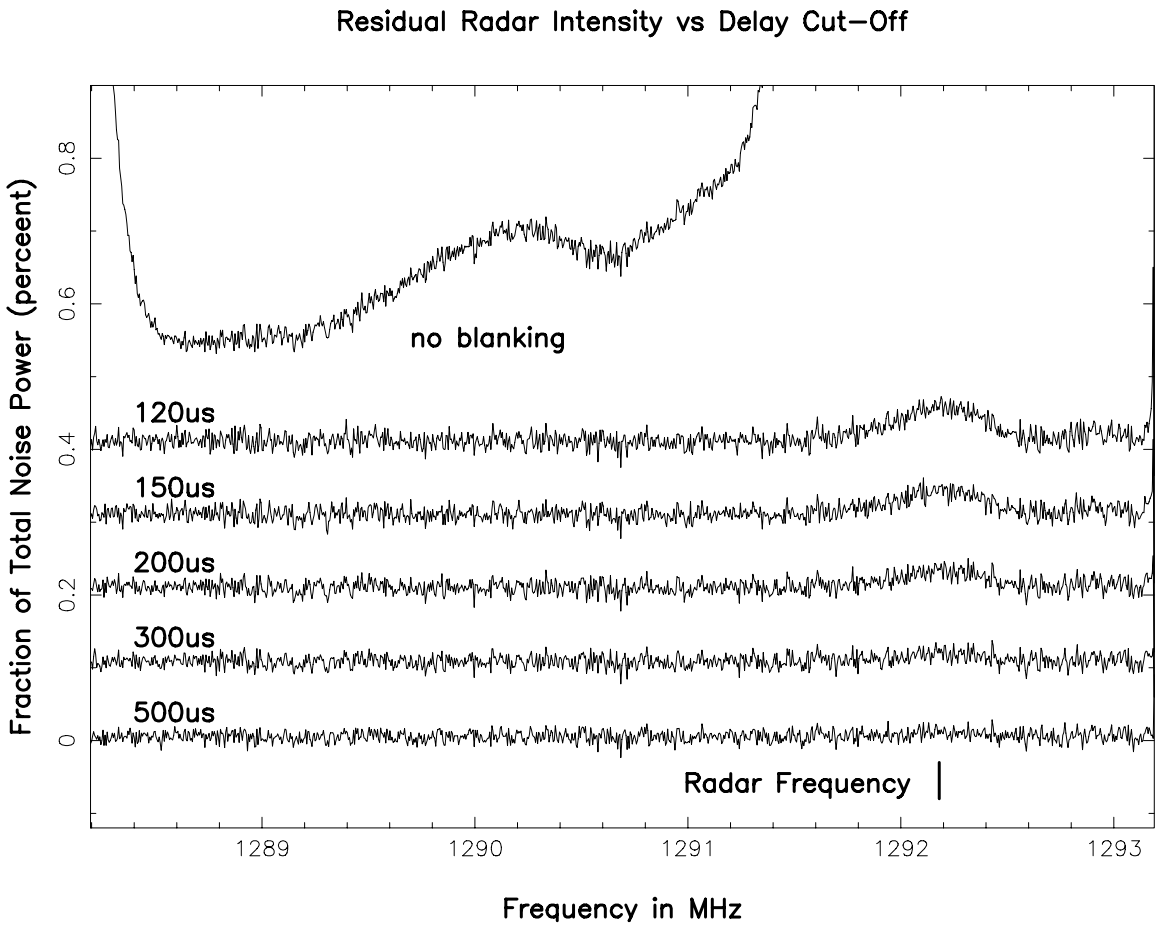

Figure 27: Residual radar signal as a function of the blanking window delay cutoff. Spectra are integrated for all 120 minutes of UGC 4288 data. The plots show the difference between spectra using various blanking window cutoff delays and the spectrum integrated using 999 μs cutoff divided by the 999-μs-cutoff spectrum. All spectral use a blanking window start of $-5\mu s$. The spectra were convolved with a 5-channel rectangular function to a resolution of 25 kHz (5.8 km/s)

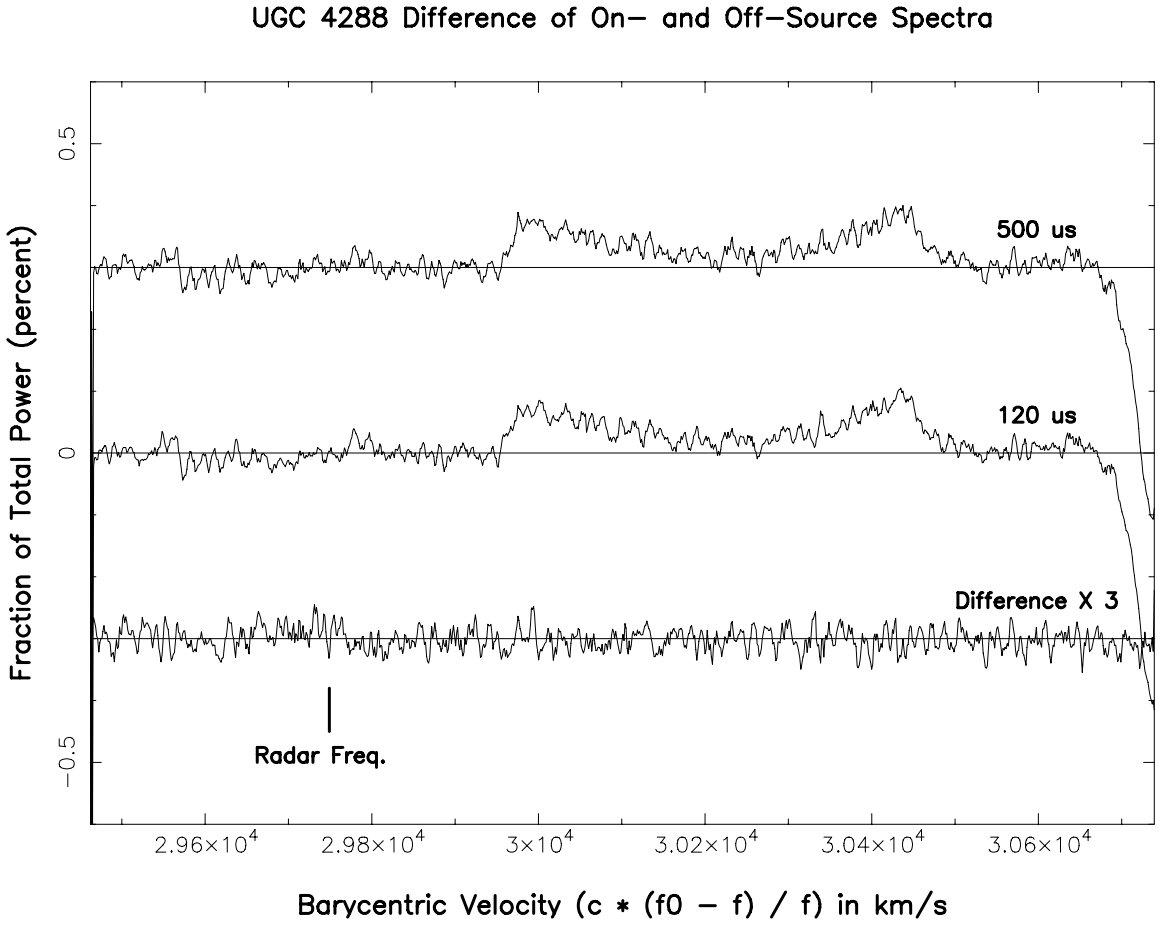

Figure 28: Comparison of (on - of) / off spectra using 500 and 120 μs blanking window cutoffs in the top and middle plots, respectively. The bottom plot is the difference of the top two with the vertical scale expanded by a factor of 3. The 120-μs spectrum is the same as the "Average" spectrum shown in Figure 25. The spectra were convolved with a 5-channel rectangular function to a resolution of 25 kHz (5.8 km/s).

References

[Carbognani *et al (2001)]* Carbognani, A., De Meyere, M., Foschini, L., Steyaert, C. 2001, On the meteor height from forward scatter radio observations, arXiv:astro-ph/0112375v1, 16 December 2001.

[O'Neil *et al (2004)]* O'Neil, K., Bothun, G., van Driel, W., Ragaigne, D. M. 2006, A New HI Catalog of Low Surface Brightness Galaxies out to z=1.0, arXiv:astro-ph/0406505 v1 23 Jun 2004

[Stennes (2001)] Stennes, M. 2001, L-Band RFI, 1256 and 1292 MHz, Handwritten Memo dated January 26, 2001